ORIGINAL ARTICLE

Molecular Plant Pathology **WILEY**

AtHVA22a, a plant-specific homologue of Reep/DP1/Yop1 family proteins is involved in turnip mosaic virus propagation

Mingshuo Xue[1] | **Luc Sofer**[1] | **Vincent Simon**[1] | **Nathalie Arvy**[1] | **Mamoudou Diop**[2] | **Roxane Lion**[1] | **Guillaume Beucher**[1] | **Amandine Bordat**[1] | **Jens Tilsner**[3,4] | **Jean-Luc Gallois**[2] 🄳 | **Sylvie German-Retana**[1] 🄳

[1]Univ. Bordeaux UMR 1332, Biologie du Fruit et Pathologie, INRAe, Equipe de Virologie, Villenave d'Ornon Cedex, France

[2]UR 1052, INRAe, GAFL Domaine St Maurice, Montfavet Cedex, France

[3]Cell and Molecular Sciences, James Hutton Institute, Dundee, UK

[4]Biomedical Sciences Research Complex, University of St Andrews, St Andrews, UK

Correspondence
Sylvie German-Retana, Univ. Bordeaux UMR 1332, Biologie du Fruit et Pathologie, INRAE, Equipe de Virologie, 71 avenue Edouard Bourlaux, CS 20032, Villenave d'Ornon Cedex 33882, France.
Email: sylvie.german-retana@inrae.fr

Funding information
Agence Nationale de la Recherche, Grant/Award Number: ANR PotyMove ANR-16-CE20-0008-01 and ANR-10-INBS-04

Abstract

The movement of potyviruses, the largest genus of single-stranded, positive-sense RNA viruses responsible for serious diseases in crops, is very complex. As potyviruses developed strategies to hijack the host secretory pathway and plasmodesmata (PD) for their transport, the goal of this study was to identify membrane and/or PD-proteins that interact with the 6K2 protein, a potyviral protein involved in replication and cell-to-cell movement of turnip mosaic virus (TuMV). Using split-ubiquitin membrane yeast two-hybrid assays, we screened an *Arabidopsis* cDNA library for interactors of ^{TuMV}6K2. We isolated AtHVA22a (*Hordeum vulgare abscisic acid responsive gene 22*), which belongs to a multigenic family of transmembrane proteins, homologous to Receptor expression-enhancing protein (Reep)/Deleted in polyposis (DP1)/Yop1 family proteins in animal and yeast. HVA22/DP1/Yop1 family genes are widely distributed in eukaryotes, but the role of HVA22 proteins in plants is still not well known, although proteomics analysis of PD fractions purified from *Arabidopsis* suspension cells showed that AtHVA22a is highly enriched in a PD proteome. We confirmed the interaction between ^{TuMV}6K2 and AtHVA22a in yeast, as well as in planta by using bimolecular fluorescence complementation and showed that ^{TuMV}6K2/AtHVA22a interaction occurs at the level of the viral replication compartment during TuMV infection. Finally, we showed that the propagation of TuMV is increased when AtHVA22a is overexpressed in planta but slowed down upon mutagenesis of *AtHVA22a* by CRISPR-Cas9. Altogether, our results indicate that AtHVA22a plays an agonistic effect on TuMV propagation and that the C-terminal tail of the protein is important in this process.

KEYWORDS
6K2 vesicles, AtHVA22a, endoplasmic reticulum, movement, plasmodesmata, potyvirus, propagation, viral replication compartment

---

Mingshuo Xue and Luc Sofer contributed equally to this work.

1 | INTRODUCTION

The cell-to-cell movement of plant viruses is a key step of the viral infection, considered as a major putative obstacle to viral exponential expansion in the plant by generating population bottlenecks (Gutiérrez et al., 2015; Miyashita & Kishino, 2010; Monsion et al., 2008) and thus, an excellent target for resistance. Indeed, a malfunction of plant factors required by the virus for its cell-to-cell movement would cause the virus to be confined or restricted to its primary infection focus, thus delaying or preventing its systemic spreading. Also, by increasing the genetic drift, reduced cell-to-cell virus movement could increase resistance durability (Quenouille et al., 2013). To invade the whole plant after replication, plant viruses move intracellularly to reach the plasmodesmata (PD), the symplastic tunnels between cells that are the gateway for this movement, then cross them to enter neighbouring cells, and eventually into sieve elements where they are transported within the source-to-sink flow of photo-assimilates (Schoelz et al., 2011). PD are structures unique to plants, crucial for the communication between the cells for plant growth, development and defence (Reagan & Burch-Smith, 2020). The deposition and breakdown of callose in the cell wall at the neck regions of PD modulates their permeability and size exclusion limit (SEL; Benitez-Alfonso et al., 2010; German et al., 2023). Despite the symplastic continuity between cells, the SEL of PD constitutes a physical barrier that must be overcome by a virus to successfully move from cell to cell. Plant virus genomes encode a class of proteins called movement proteins (MP) that interact with host proteins to modify the PD for cell-to-cell transportation of the viral genome (Heinlein, 2015; Kumar & Dasgupta, 2021).

The *Potyvirus* genus is one of the largest genera of plant viruses responsible for serious diseases in vegetable and fruit crops (Inoue-Nagata et al., 2022; Wylie et al., 2017). However, the cell-to-cell movement mechanism of potyviruses is far from being understood. Numerous genetic, cellular and ultrastructural studies have highlighted how the potyvirus transport involves a large network of interactions with viral and cellular proteins (Martínez-Turiño & García, 2020; Solovyev et al., 2022; Wang, 2021). However, whether potyviruses move between cells as virions or other movement complexes such as ribonucleoprotein or vesicular viral replication complexes still remains an unsolved question (Xue et al., 2023). Furthermore, the discovery of viral vesicles present in the apoplastic space during turnip mosaic virus (TuMV) infection, suggesting a move in the extracellular space, adds another layer of complexity to potyvirus transport (Movahed, Cabanillas, et al., 2019; Wan & Laliberté, 2015).

In particular, there is no dedicated MP for potyviruses. Reverse genetics and cell biological studies have shown that four potyviral proteins constitute the multicomponent core transport system of potyviruses (reviewed in Revers & García, 2015; Wang, 2021, Xue et al., 2023). The P3N-PIPO ('P3-N-terminal-Pretty Interesting Potyviridae Open Reading Frame') displays MP-related functions as it spreads between cells, thus seeming capable of increasing the PD SEL (Cheng et al., 2017; Chung et al., 2008; Cui et al., 2017; Wen

& Hajimorad, 2010; Vijayapalani et al., 2012). The cylindrical inclusion helicase (CI) is crucial for replication and movement (Deng et al., 2015; Movahed et al., 2017; Sorel et al., 2014), together with the structural capsid protein (CP; Martínez-Turiño & García, 2020; Wang, 2021). The targeting of CI to PD is mediated by P3N-PIPO (Wei, Zhang, et al., 2010), which itself is targeted to the plasma membrane through an interaction with the host plasma membrane-associated protein PCaP1 (Vijayapalani et al., 2012). The fourth potyviral 'MP' protein, the second '6 kDa molecular-weight membrane anchoring protein' (6K2), induces the formation of endoplasmic reticulum (ER)-derived vesicles involved in replication and movement (Beauchemin & Laliberté, 2007; Grangeon et al., 2012, 2013). When expressed alone (in the absence of virus infection), the 6K2 protein can induce vesicles that are morphologically identical to those observed in infected cells (González et al., 2019; Grangeon et al., 2013). TuMV infection leads to drastic rearrangements of the early secretory pathway of the cell, including a perinuclear globular-like structure composed of an amalgamation of ER, Golgi bodies, coat protein complex II (COPII) coatamers and chloroplasts (Grangeon et al., 2012; Wei, Huang, et al., 2010). This perinuclear globular structure contains viral RNA, as well as viral proteins involved in replication (Cronin et al., 1995; Cui et al., 2010; Cui & Wang, 2016; Klein et al., 1994; Lõhmus et al., 2016; Martínez-Turiño & García, 2020; Wei, Huang, et al., 2010), together with host translation factors (Beauchemin & Laliberté, 2007; Dufresne et al., 2008; Lõhmus et al., 2016; Thivierge et al., 2008). Besides this large perinuclear structure, that can be considered as the viral replication compartment (VRC), motile 6K2-vesicles located at the cell periphery are observed and derive from the perinuclear structure (Grangeon et al., 2012). The intracellular motility of potyvirus 6K2-vesicles relies on both early secretory pathway and the actin network and the 6K2 vesicles have been shown to be mobile between cells (Grangeon et al., 2012, 2013; Movahed et al., 2017). Therefore, a tight coupling between replication and cell-to-cell movement occurs during potyvirus movement, as demonstrated for other plant viruses (Tilsner et al., 2013).

A few plant factors involved in potyvirus intra- and intercellular movement have been identified so far, including plasma membrane (PM)-associated proteins targeted to PD (Geng et al., 2015; Park et al., 2017; Rocher et al., 2022; Vijayapalani et al., 2012), proteins involved in endomembrane remodelling, ER bending, interorganelle vesicular exchanges (Cabanillas et al., 2018; Cui et al., 2018; Jiang et al., 2015; Movahed, Sun, et al., 2019; Uchiyama et al., 2014) and proteins involved in endocytic processes (Wu et al., 2020, 2022).

Among host factors involved in potyvirus movement, only a few are PD located. The interactions between PCaP1 and P3N-PIPO, or StREM1.3 and CI for example, occur at the PD levels but also outside of the PD at the PM (Rocher et al., 2022; Vijayapalani et al., 2012). The PD-located *Nicotiana benthamiana* α-expansin, NbEXPA1, when ectopically expressed, promotes TuMV replication and intercellular movement, suggesting that this PD-specific cell wall loosening protein could be involved in PD modification to facilitate potyviral cell-to-cell movement (Park et al., 2017). The synaptotagmin SytA

localizes to sites where ER makes contact sites with PM such as at the PD, and could play a role in the way P3N-PIPO could be directed to PD although no direct interaction between P3N-PIPO and SytA protein has been described so far (Uchiyama et al., 2014).

In this study, we aimed at identifying plant factors involved in potyvirus cell-to-cell movement, by focusing on the role of PD in this process. As potyviruses have developed strategies to hijack the host secretory pathway and PD for their transport, and as the 6K2 is a key viral protein in this process, the goal was to identify membrane and/or PD proteins that interact with the 6K2. We used a split-ubiquitin yeast two-hybrid (Y2H) screen to identify AtHVA22a (*Hordeum vulgare abscisic acid responsive gene 22*) that interacts with the 6K2 of TuMV. AtHVA22a belongs to a multigenic family of transmembrane proteins, homologous to Receptor expression-enhancing protein (Reep)/Deleted in polyposis (DP1)/Yop1 family proteins in yeast and mammals (Chen et al., 2002). The role of HVA22 proteins in plants is still not well known, although proteomics analysis of PD fractions purified from *Arabidopsis* suspension cells show that HVA22a is highly enriched in an *Arabidopsis* PD proteome (Brault et al., 2019). In this study we show that AtHVA22a represents a new plant protein required for efficient infection by potyviruses.

2 | RESULTS

2.1 | ^{TuMV}6K2 interacts with AtHVA22a in yeast cells and in planta

The split-ubiquitin membrane Y2H assay (SuY2H) (DUALmembrane system) was used to identify any membrane and/or PD-associated proteins interacting with the viral bait ^{TuMV}6K2. This approach is especially relevant as TuMV replicates in VRCs derived from the ER, which is intimately involved in trafficking cellular macromolecules and the core component of the endomembrane system. Importantly, we performed preliminary assays to determine whether ^{TuMV}6K2 bait is functional for the DUALmembrane SuY2H assay (Figure S1a). Indeed, ^{TuMV}6K2-Cub bait is properly inserted into the yeast membrane with the Cub moiety located on the membrane cytosolic side and does not auto-activate the system (Figure S1a). A cDNA library from *Arabidopsis thaliana* (Bernard et al., 2012) was screened with ^{TuMV}6K2 as bait as described in the Experimental Procedures section, and 252 positive clones were isolated on selective −2HTL medium. The corresponding prey vector cDNAs were PCR amplified from the 252 colonies and digested with the restriction enzyme MseI. We classified the clones into 21 groups according to the size of the insert and MseI-digestion profiles and 75 clones (up to four clones per group) were sequenced. A list of 61 unique ID potential candidate proteins was established (Table S1). This list was compared to published PD proteome data (Brault et al., 2019; Grison et al., 2015; Salmon & Bayer, 2013). We therefore refined and selected a list of 26 candidates (Table S1) according to their PD location and/or membrane association. Eleven of these candidates were chosen to perform confirmation assays of the interactions with ^{TuMV}6K2

via a targeted SuY2H assay. Among the seven non-autoactivators, AtHVA22a (*Arabidopsis thaliana Hordeum vulgare abscisic acid responsive gene 22*, TAIR accession AT1G74520; Chen et al., 2002) is a protein that is highly enriched in the *Arabidopsis* PD proteome (Brault et al., 2019). Therefore, this 6K2 interactor was chosen for further investigation. In our targeted SuY2H assay, yeast transformants expressing ^{TuMV}6K2 bait in combination with the rescued prey plasmid encoding AtHVA22a grew on high-stringency selective medium (–AHTL) supplemented with 1 mM 3-amino-1,2,4-triazole (3-AT), confirming the protein–protein interaction (Figure 1a).

We assessed the interaction between AtHVA22a and ^{TuMV}6K2 in planta using bimolecular fluorescence complementation (BiFC) assays in *Nicotiana benthamiana* leaves. To this end, chimeric constructs expressing 6K2 fused to the N-terminal half of the yellow fluorescent protein (nYFP-6K2) and AtHVA22a fused to the C-terminal half of YFP (HVA22a-cYFP) were transiently co-expressed via agroinfiltration, and fluorescence was detected by confocal microscopy. The expression of each fusion protein was confirmed by western blot (Figure S1b). As shown in Figure 1b, AtHVA22a interacted with ^{TuMV}6K2. The YFP fluorescence signal was detected in the experimental samples 3–4 days after agroinfiltration in more than 15 independent experiments, whereas it was not detected in the negative controls (i.e., only nYFP-6K2 or HVA22a-cYFP expressed alone or nYFP-6K2 expressed with P3N-PIPO-cYFP, a negative control based on Movahed et al., 2017; Figure S1b). The lambda scan mode confirmed that a maximum of fluorescence emission is observed at 530 nm, which corresponds to YFP emission wavelength (Figure S1b). The original western blots are available in the Figures WB1 and WB2. As a positive control, we used the combination nYFP-6K2 + cYFP-StREM1.3, the REMORIN protein that localizes in plasma membrane nanodomains (Rocher et al., 2022). This interaction occurred at the level of the PM (Figure S1b), whereas the YFP signal resulting from ^{TuMV}6K2/AtHVA22a interaction was observed as dots in close association with BFP-HDEL ER labelling (Figure 1b), and in very close proximity with 6K2-RFP-labelled vesicles when co-expressed during BiFC experiment (Figure 1b, Movie S1). We never observed a clear PD localization of ^{TuMV}6K2/AtHVA22a interaction signal although some proximity with PD callose-binding protein 1 (Simpson et al., 2009; PDCB1-mcherry) PD marker was reproducibly observed (Figure S1c).

2.2 | Identification of structural domains of AtHVA22a

AtHVA22a protein belongs to the multigene *HVA22* family (Chen et al., 2002; Shen et al., 1993, 2001), which gathers plant homologues of proteins responsible for the constriction of ER tubules in mammals and yeast, the Reep/DP1/Yop1 family (Chen et al., 2002). Yop1 regulates vesicle trafficking in stressed yeast cells (Brands & Ho, 2002). However, the role of HVA22 gene family proteins is very poorly known in plants, besides their potential involvement in autophagy and dormancy (Chen et al., 2009), response
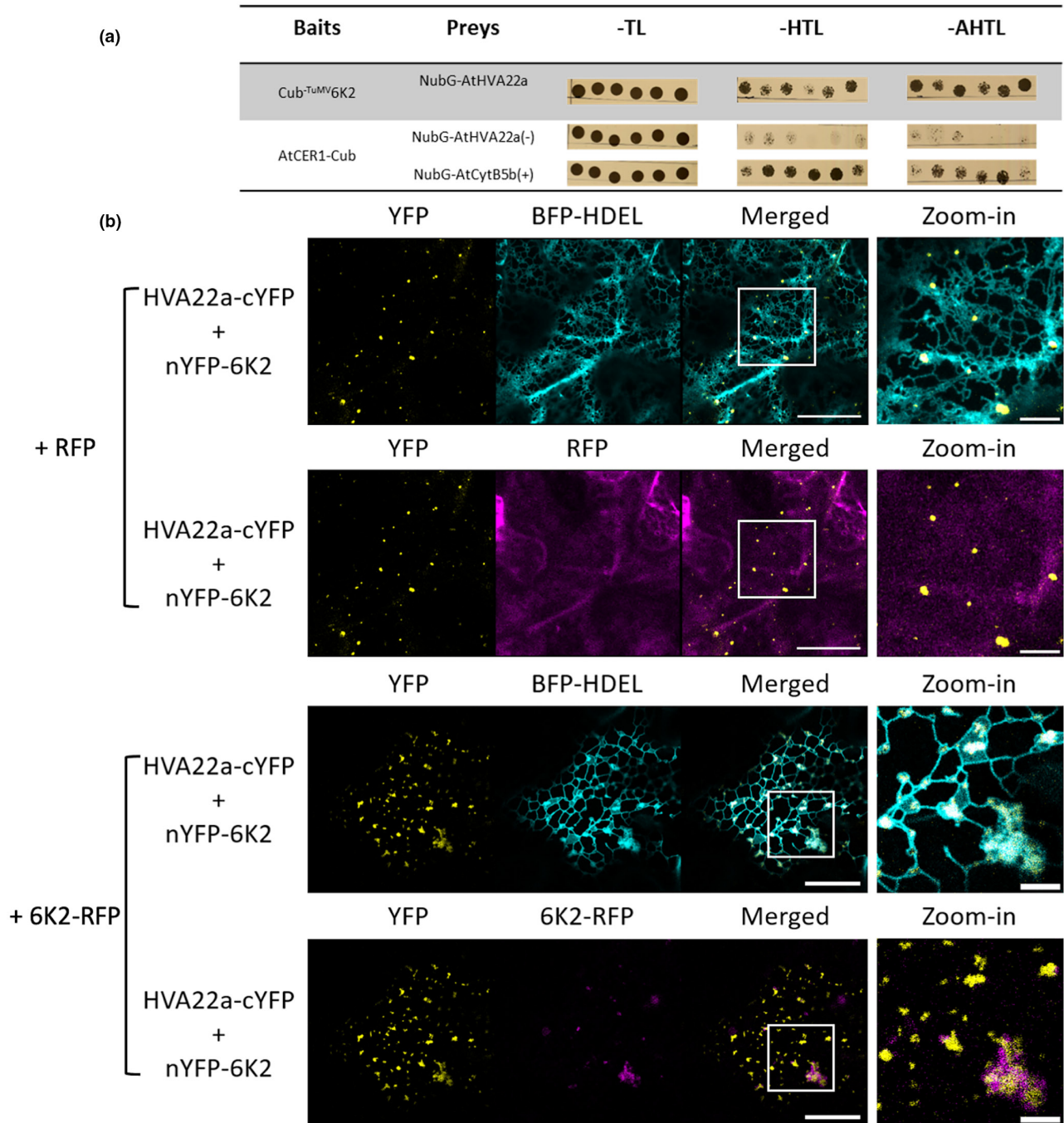
FIGURE 1 ^{TuMV}6K2 interacts in yeast and in planta with AtHVA22a. (a) Interaction between ^{TuMV}6K2 and AtHVA22a in split ubiquitin yeast two-hybrid assay. Six independent yeast colonies co-transformed with NubG-AtHVA22a and Cub-^{TuMV}6K2 resulted in vigorous growth on medium containing 1 mM 3-amino-1,2,4-triazole (3-AT) and lacking Leu, Trp, His and Ade (−AHTL). (b) Bimolecular fluorescence complementation (BiFC) detection of the interaction between nYFP-6K2 and HVA22a-cYFP in *Nicotiana benthamiana* epidermal cells. The YFP signal resulting from ^{TuMV}6K2–HVA22a interaction is observed as dots in close association with endoplasmic reticulum (ER) labelling (BFP-HDEL) and in very close proximity with 6K2-RFP-labelled vesicles. Images are single confocal sections of *N. benthamiana* epidermal cells co-expressing HVA22a-cYFP+nYFP-6K2 with free RFP or 6K2-RFP fusion together with BFP-HDEL. The merges of the YFP signal with BFP or RFP are shown separately and correspond to the same cell where the three fluorochromes are expressed. Images were captured at 2 days post-infiltration (dpi). Insets (Zoom-in) are boxed in the corresponding original images. Scale bars: 20 μm and 5 μm for 'Zoom-in' images.

to abiotic stresses (Chen et al., 2002; Gomes Ferreira et al., 2019; Wai et al., 2022) and in plant immunity towards fungal infection in rice (Meng et al., 2022). In *Arabidopsis*, 11 HVA22 homologues, designated AtHVA22a to k, can be separated into four subfamilies, with AtHVA22a, b and c grouped in the group 1 (Figure S2a,b). Based on amino acid sequence alignments, the N-terminal half of

the protein is more conserved than the C-terminal one. Among the HVA22 family in *Arabidopsis*, only the two closely related members AtHVA22a and ATHVA22c are highly enriched in a PD proteome (Brault et al., 2019). By performing protein structure prediction with AlphaFold and Phyre 2 (Jumper et al., 2021; Kelley et al., 2015) the 177 amino acids (aa) long AtHVA22a sequence can be split into two main parts. The N-terminal half (aa 1–95) encompasses three trans-membrane helices (hereafter termed HVA22aTMD) and includes a pre-dicted reticulon homology domain (that consists of two hydrophobic transmembrane segments separated by a hydrophilic loop that can form a hairpin within the lipid bilayer and act as a wedge structure; Figure S2c). The HVA22aTMD domain is followed by a C-terminal hy-drophilic tail (termed HVA22aC-ter, aa 96–177) including a potential amphipathic helix (APH). In yeast Yop1, the TMD mediates homo-oligomerization, whilst for membrane constriction an APH in the C-terminal cytoplasmic domain is essential (Brady et al., 2015). Our predictions suggest that the AtHVA22a structure differs from some of the proteins of the DP1/Yop1 and reticulon (RTN) families in yeast and animals, which have four transmembrane helices with both ter-mini facing the cytoplasm (Brady et al., 2015; Sparkes et al., 2010; Voeltz et al., 2006). However, according to Xiang et al. (2023), REEP1, the mammal homologue of HVA22 (Angelotti, 2022; Brands & Ho, 2002), which belongs to REEP1-4 subfamily that is a part of the DP1/Yop1p family, may have also three transmembrane domains with a C-terminal cytoplasmic domain and a N-terminal oriented towards the ER lumen (Fan et al., 2022) comparable to predicted AtHVA22a topology.

2.3 | Fluorescent reporter fusions of AtHVA22a show ER and partial PD localization

As AtHVA22a was found to be highly enriched in the PD proteome (Brault et al., 2019), we assessed the subcellular localization of AtHVA22a fusions to fluorescent reporters following transient ex-pression under the control of the cauliflower mosaic virus 35S pro-moter in *N. benthamiana*. By fusing the GFP at the N-terminus of AtHVA22a, the GFP-HVA22a fusion protein showed ER labelling (Figure 2a) and a partial PD labelling was observed using aniline blue staining of callose (β-1,3-glucan), a structural and functional component of PD (Figure 2b). GFP-HVA22a signal was observed at PD entrance rather than completely traversing through the chan-nels, but due to diffraction-limited imaging it is hard to confirm this observation. Compared to the situation where a PD marker protein (PD callose-binding protein 1, PDCB1) (Simpson et al., 2009) is co-expressed with aniline blue staining, the percentage of co-labelled spots between GFP-HVA22a and aniline blue was significantly lower (Figure 2c) but higher than free GFP, confirming that GFP-HVA22a is partially located at PD. GFP-HVA22a PD association did not seem to be modified during TuMV/6K2:mCherry infection (Figure 2b,c). On the other hand, the C-terminal fusion AtHVA22a-GFP showed very faint ER labelling and mainly formed punctae, some of them displaying PD localization as shown by colocalization with the PD

marker MCTP6 (Figure 2d). Interestingly, when AtHVA22a-GFP was co-expressed with a heterologous MP (cucumber mosaic virus 3a MP) a clear PD localization of the HVA22a-GFP fusion was observed (Figure 2e).

By splitting the HVA22aTMD and HVA22aC-ter domains of AtHVA22a, we observed that both N-terminal and C-terminal GFP fusions of HVA22aTMD localized to the ER (Figure S3A), without ob-vious PD localization. The HVA22aC-ter tail, which includes the region homologous to the yeast Yop1 APH (amino acids 95–107 in HVA22a), was both cytoplasmic and also showed PD association, which was in-creased during TuMV/6K2:mCherry infection (Figure S3b,c).

Using the RaptorX web server (Zeng et al., 2018), we predicted that the transmembrane domains 1 and 3 in HVA22aTMD might be involved in the interaction with TuMV6K2. By performing bimolecular fluorescence complementation (BiFC) experiments, we confirmed that HVA22aTMD interacts with TuMV6K2 (Figure S3d). It must be stressed that the YFP signal resulting from the interaction labels the ER tubules and differs from the YFP signal observed when the full-length AtHVA22 interacts with TuMV6K2 (Figure S3d, Figures WB3 and WB4). Therefore, the N-terminal region of AtHVA22a is in-volved in the interaction with TuMV6K2, but the lack of the C-terminal cytoplasmic tail of AtHVA22a modifies the subcellular localization of the interacting partners just as it does for the HVA22a GFP fusions as well. We also performed BiFC experiments to check whether the HVA22aC-ter tail interacts with TuMV6K2. No fluorescence was observed for HVA22aC-ter-cYFP/nYFP-6K2 and HVA22aC-ter-nYFP/cY-FP-6K2 combinations, and the expression of HVA22aC-ter-nYFP and 6K2 fusion proteins was confirmed by western blot (Figure S3d). Those results suggest that the HVA22aC-ter domain is not directly in-volved in the interaction with 6K2.

Based on all those observations, AtHVA22a is an ER protein that displays partial PD association. The C-terminal cytoplasmic tail is not essential for the interaction of AtHVA22a with TuMV6K2, but in its absence the interacting partners remain ER located. This HVA22aC-ter tail also displays some PD association that is increased during TuMV-6K2-mCherry infection.

2.4 | AtHVA22a interacts with TuMV6K2 at the level of the VRCs during TuMV infection

Although we observed in yeast and in planta an interaction be-tween TuMV6K2 and AtHVA22a, when those two proteins were co-expressed in *N. benthamiana* as either C- or N-terminal fu-sions, a close proximity was observed with the two proteins able to move in concert but no clear overlapping of fluorescent signals (Figure S4, Movies S2 and S3). Both SuY2H and BiFC systems allow us to stabilize and detect otherwise transient interactions. In order to capture the TuMV6K2/AtHVA22a interaction during TuMV infec-tion, a more biologically relevant situation when viral proteins are expressed from the viral genome, we used the TuMV/6K2:mCherry construct (Jiang et al., 2015) where the genome of TuMV is engi-neered to ectopically express the mCherry fluorescent protein fused
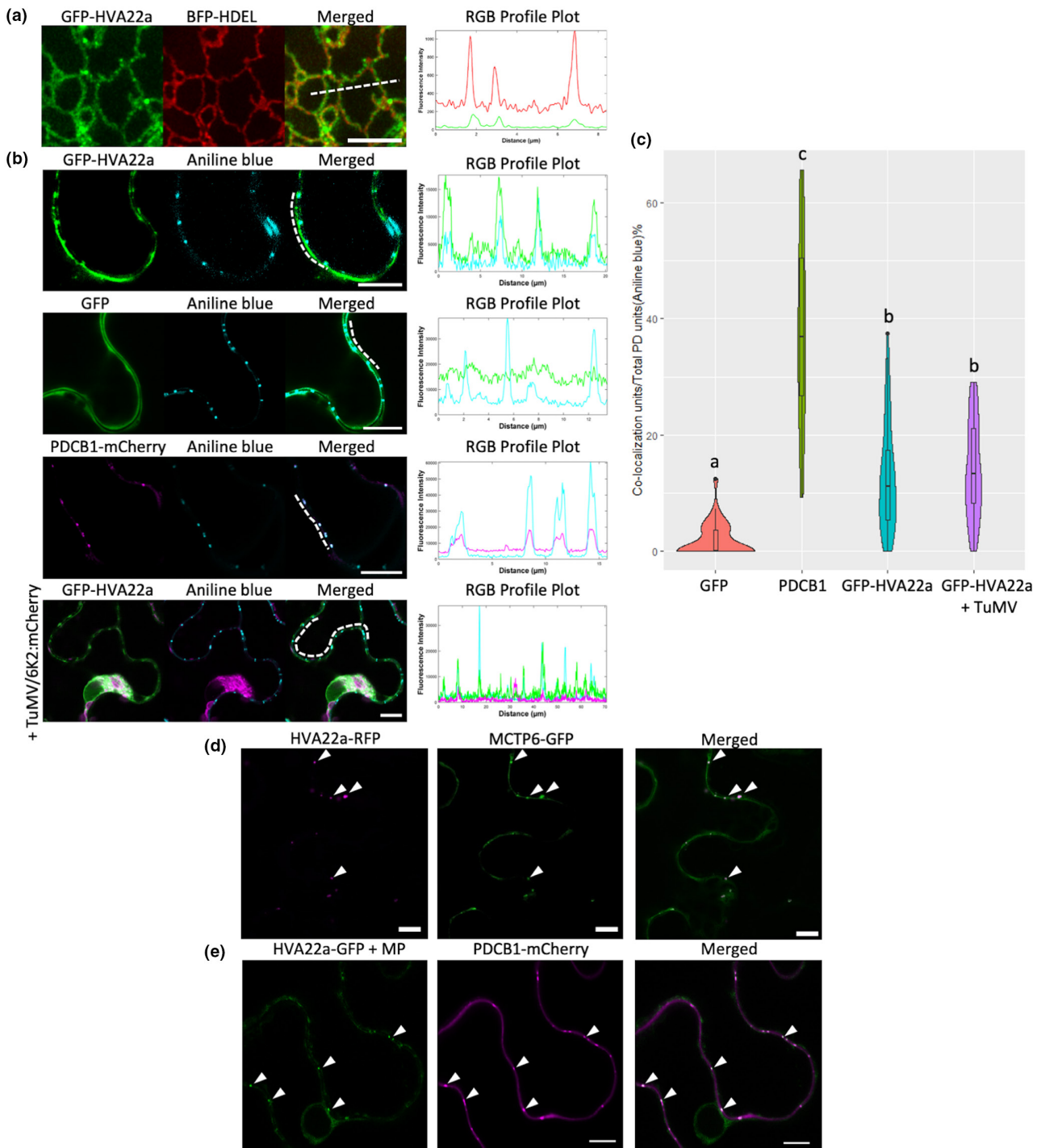
FIGURE 2 HVA22a is an endoplasmic reticulum (ER)-associated protein with some plasmodesmata (PD) localization. (a) Confocal images of *Nicotiana benthamiana* epidermal cells co-expressing GFP-HVA22a with the ER marker BFP-HDEL at 3 days post-infiltration (dpi). Scale bar: 5 μm. (b) Aniline blue staining of callose deposition at the PD pit fields in *N. benthamiana* leaf cells expressing GFP-HVA22a, GFP, PCDB1-mCherry or GFP-HVA22a in TuMV/6K2:mCherry infected cells at 3 dpi. Intensity plots along the white dashed lines in the merged images are shown for each colocalization pattern. All images are taken at 3 dpi. Scale bars: 10 μm. (c) Partial colocalization between PD pit fields (indicated by aniline blue staining) and GFP-HVA22a signal. PDCB1-mCherry is the positive PD marker (positive control), whereas GFP is the negative control. Between 15 to 47 images were analysed for each condition, corresponding to 636–1653 PD pit fields. A statistical analysis was performed using the % of colocalization value, using Kruskal–Wallis test. (d) Confocal images of *N. benthamiana* epidermal cells co-expressing HVA22a-RFP with MCTP6-GFP. (e) Confocal images of *N. benthamiana* epidermal cells co-expressing HVA22a-GFP with PDCB1-mCherry and the heterologous movement protein (MP) from cucumber mosaic virus (CMV3a-Flag). Images were captured at 3 dpi. White arrowheads indicate PD localization. Scale bars: 10 μm.

at the C-terminus of the 6K2. This allows us to visualize the TuMV-produced 6K2-mCherry vesicles labelling the VRCs and mobile 6K2-vesicles in the infected cells. Figure 3 shows that both HVA22a-GFP (Figure 3a) and GFP-HVA22a (Figure 3b) were localized at the ^{TuMV}6K2-labelled VRC during TuMV infection (see also Movies S4 and S5). Figure 3c shows that unfused GFP was not localized at the VRC during TuMV/6K2:mCherry infection and Figure 3d shows that no modification of the subcellular localization of GFP-HVA22a occurred during unfused RFP co-expression. Furthermore, by performing BiFC during TuMV infection, we also observed that the YFP signal resulting from HVA22a-cYFP/nYFP-^{TuMV}6K2 interaction was also strongly associated with the VRC (Figure 3e). In conclusion, during TuMV infection, AtHVA22a interacts with ^{TuMV}6K2 at the level of the 6K2-induced VRC.

2.5 | *AtHVA22a* overexpression increases TuMV propagation in *N. benthamiana*

To assess a biological role of the interaction observed between ^{TuMV}6K2 and AtHVA22a, we investigated the impact of transient overexpression of AtHVA22a on the ability of TuMV-GFP to spread in the inoculated leaves of *N. benthamiana*. The expression and subcellular localization of HVA22a fluorescent fusions were examined by confocal microscopy and confirmed by western blot (Figure 4a, Figure WB5). The transient overexpression of AtHVA22a RFP- or 6×histidine-fusion both led to a significant increase of the area of infection foci induced by TuMV-GFP, compared to overexpression of free RFP as a negative control (Figure 4b). As a positive control, we reproducibly observed the agonistic effect of transient overexpression of StREM1.3 on TuMV propagation previously described (Rocher et al., 2022). Altogether, our results strongly suggest that AtHVA22a plays a proviral role for TuMV propagation (defined as the combined effect of replication efficiency and movement) in the inoculated leaves of *N. benthamiana*.

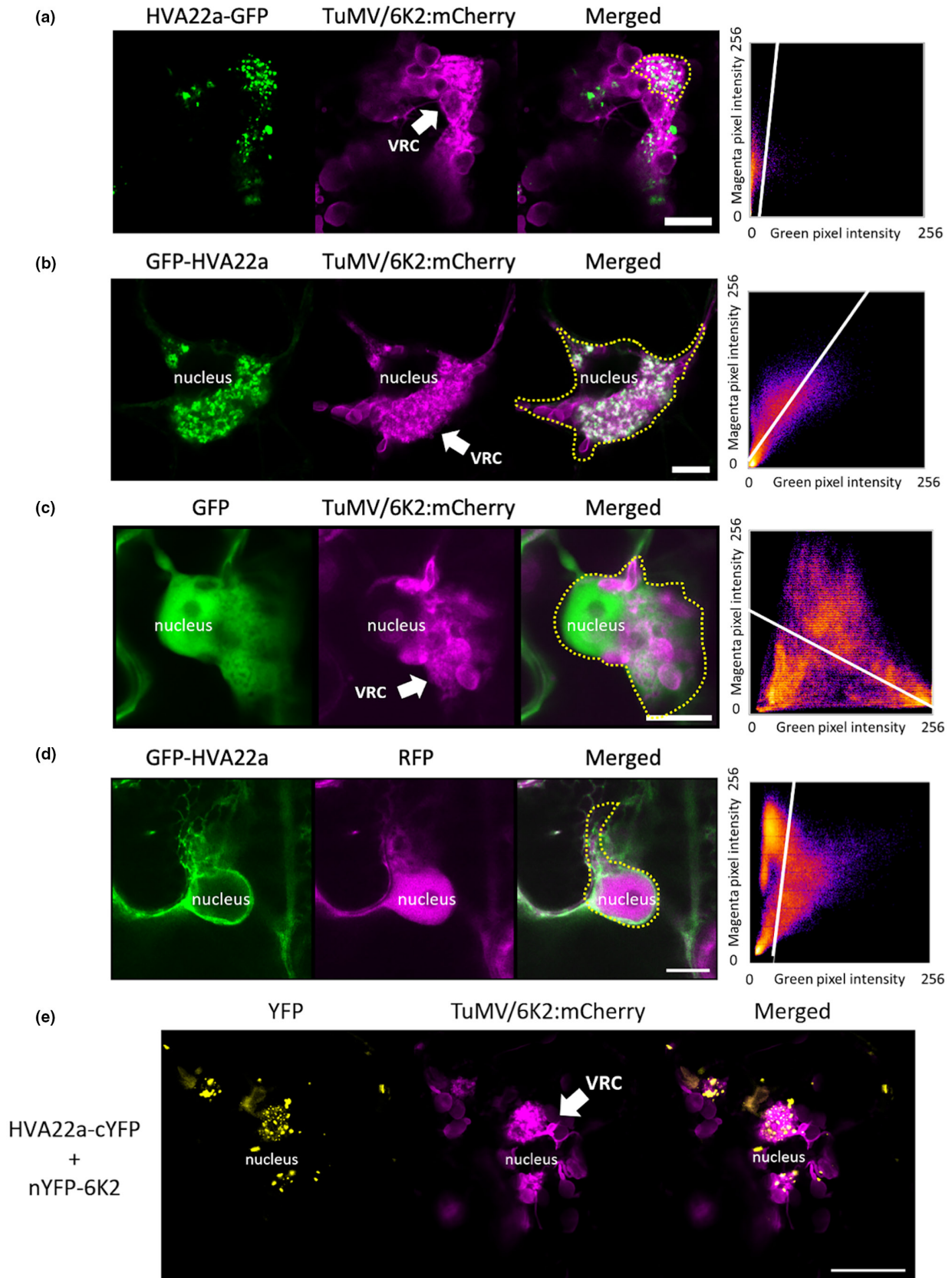## 2.6 | TuMV propagation is slowed down in *Arabidopsis AtHVA22a* CRISPR-Cas9 mutants

To study the interaction of TuMV with AtHVA22a in *Arabidopsis*, we first analysed whether TuMV infection induces a modification of the expression level of AtHVA22a, using specific reverse transcription-quantitative PCR (RT-qPCR) primers qHVA22a2-Fwd and qHVA22a2Rev (Table 1). We used the TuMV-GFP//mCherry construct to follow the viral infection and according to our results, TuMV-GFP//mCherry infection did not impact the level of expression of AtHVA22a at until 6days post-inoculation (dpi) in the inoculated leaves and 13 dpi in the systemically infected leaves (Figure S5). As overexpression of AtHVA22a increases TuMV propagation in the inoculated leaves of *N. benthamiana*, we tested if a lack of expression of AtHVA22a in *Arabidopsis* would have the opposite effect. A CRISPR-Cas9-based strategy was therefore employed and four independent

homozygous CRISPR-Cas9 mutants were obtained (Figure S6). The guide RNAs were designed in a way to avoid any off-target in the *Arabidopsis* genome. The three independent mutants, *hva22a-1*, *hva22a-2* and *hva22a-3*, display indels in the *AtHVA22a* sequence (Figure S6a,b) and are predicted to express an AtHVA22a protein containing 20 or 21 random amino acids instead of the C-terminal domain downstream of the region corresponding to the APH in the yeast homologue Yop1 (Figure 5a,b). The mutant *hva22a-4* has an in-frame deletion of two amino acids (Asn 113 and Ile 114) and its 3D structure is predicted to be less affected that the three other mutants (Figure 5b). The mutant plants did not display any difference in their morphology compared to wild-type plants (Figure 5c). To confirm the proviral role played by AtHVA22a, we surveyed TuMV-GFP//mCherry propagation in the four CRISPR-Cas9 mutants affected in the C-terminal cytoplasmic domain. Figure 5c shows that the surface of the infection foci induced by TuMV-GFP//mCherry was significantly reduced in the three independent mutants *hva22a-1*, *hva22a-2* and *hva22a-3* compared to *hva22a-WT*. In contrast, the surface of the infection foci in *hva22a-4* was similar to those in wild-type *hva22a-WT*, suggesting that the 2 aa deletion might not affect the structure and/or function of AtHVA22a for TuMV propagation. At this point, we do not have any hypothesis that could explain why the infection foci are more numerous in the *hva22a-1*, *hva22a-2* and *hva22a-3* mutants than in the wild type (WT) and *hva22a-4* (Figure 5c). We then checked the subcellular localization of the corresponding mutants through transient expression of GFP-fusions in *N. benthamiana*. In at least two independent experiments, we reproducibly observed a weaker level of GFP signal for the three mutants *hva22a-1*, *-2* and *-3* compared to *hva22a-4* and *hva22a-WT*. In Figure S7a the images corresponding to *hva22a-1*, *-2* and *-3* were acquired by increasing both the gain and the power of the argon laser. It seems that their subcellular localization did not drastically differ from hva22a-WT and was ER-associated. We confirmed, by performing a quantitative western blot analysis (Figure S7b,c), the instability of HVA22a-1, -2 and -3 proteins when transiently expressed compared to HVA22a-4 and HVA22a-WT proteins expressed in the same conditions. Therefore, the modification of the C-terminal cytosolic tail seems to decrease the stability of AtHVA22a protein when ectopically expressed in *N. benthamiana* but does not seem to affect drastically its subcellular localization when fused to GFP. Interestingly, Xiang et al. (2023) also showed that the C-terminal part of Yop1 is critical for the stability and the function of the protein.

Altogether, our results indicate that AtHVA22a plays an agonistic effect on TuMV propagation and that the C-terminal tail of the protein is important in this process.

2.7 | TuMV replication is not affected in *AtHVA22a* CRISPR-Cas9 mutants

The decreased spread of TuMV in three independent CRISPR-Cas9 *hva22a* mutants might be explained by a reduced virus replication. In order to quantify the level of accumulation of TuMV, independent

(a) HVA22a-GFP | TuMV/6K2:mCherry | Merged
(b) GFP-HVA22a | TuMV/6K2:mCherry | Merged
(c) GFP | TuMV/6K2:mCherry | Merged
(d) GFP-HVA22a | RFP | Merged
(e) HVA22a-cYFP + nYFP-6K2 | YFP | TuMV/6K2:mCherry | Merged

of the movement, we tried to isolate and transfect protoplasts as previously described (Vijayapalani et al., 2012) from leaves of WT and CRISPR-Cas9 *hva22a* mutants. However, this approach was unsuccessful. As a remediating option, we used the construct TuMV-GFP//mCherry that allows us to distinguish primary infected cells, which express both mCherry and GFP, from secondary infected cells,

FIGURE 3 HVA22a is localized at viral replication compartment (VRC) during TuMV infection. Confocal images of *Nicotiana benthamiana* epidermal cells co-expressing (a) HVA22a-GFP with TuMV/6K2:mCherry, (b) GFP-HVA22a with TuMV/6K2:mCherry, (c) unfused GFP with TuMV/6K2:mCherry, (d) GFP-HVA22a with unfused RFP. The white arrows indicate the VRC near the nucleus, induced by TuMV/6K2:mCherry infection. Scatter plots represent the correlation between green pixel intensity and magenta pixel intensity in the region of interest (ROI) indicated by yellow dotted lines. The white lines represent the slopes. Images are single confocal sections at 3 days post-infiltration (dpi). Scale bars: 10 μm. (e) The YFP signal resulting from TuMV6K2–HVA22a interaction is observed at VRC during TuMV infection. Bimolecular fluorescence complementation (BiFC) detection of interaction between nYFP-6K2 and HVA22a-cYFP in *N. benthamiana* epidermal cells infected by TuMV/6K2:mCherry at 3 dpi. The white arrow indicates the VRC near the nucleus, induced by TuMV/6K2:mCherry infection. Scale bar: 20 μm.
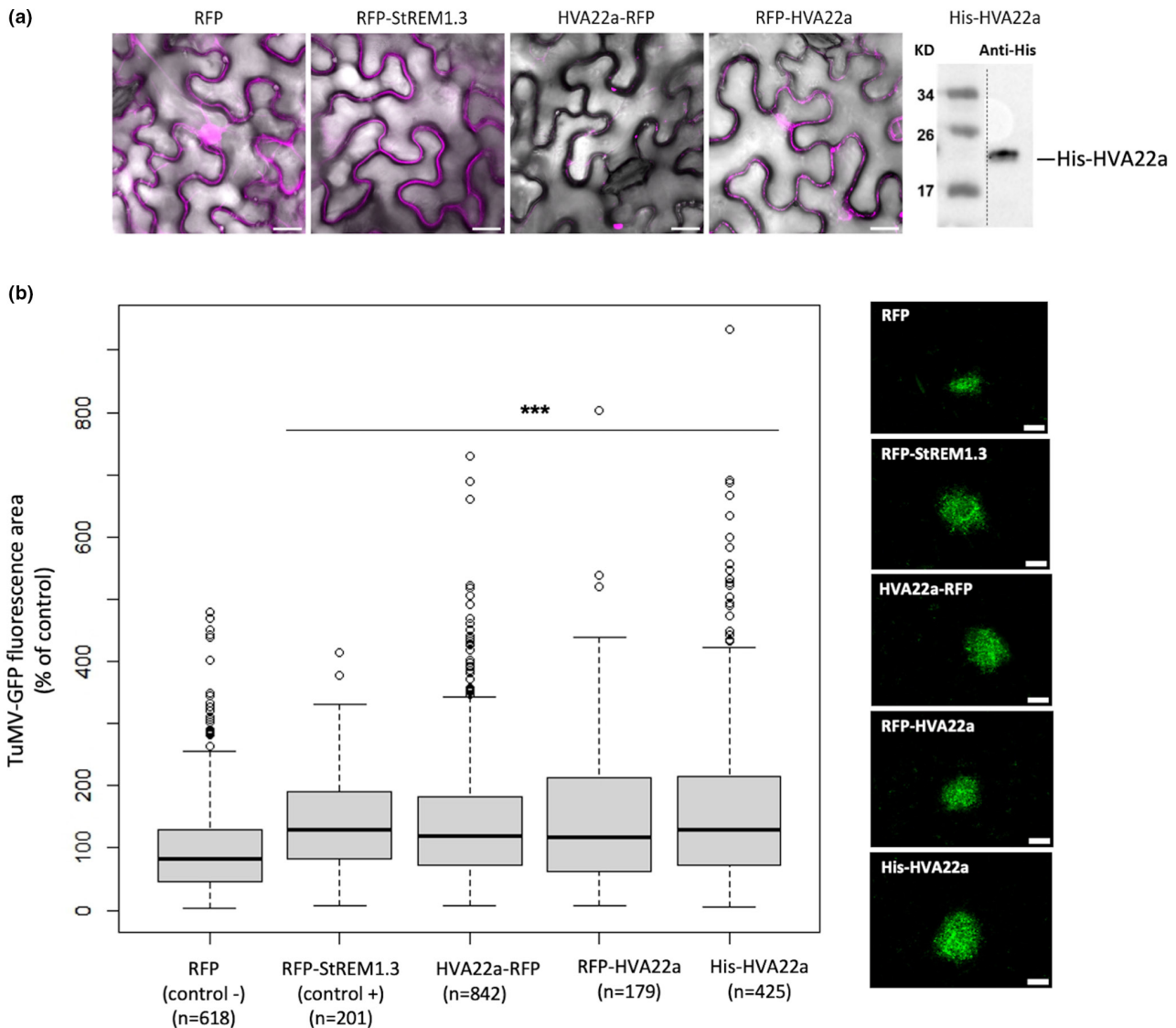

FIGURE 4 HVA22a transient overexpression increases TuMV-GFP propagation in *Nicotiana benthamiana*. (a) Confocal microscopy images representative of the subcellular localization of transiently expressed RFP 4 days after agroinfiltration. Confirmation of His-HVA22a protein expression by western blot (WB) using anti-His antibody at 5 days post-infiltration. The dotted line in the WB indicates that lanes were stitched, the original membrane is shown in the Figure WB5. Scale bars: 20 μm (b) The areas of the GFP infection foci are normalized and expressed in % of the area of TuMV-GFP propagation in the absence of HVA22a (free RFP negative control). Statistical analysis: one-way analysis of variance (ANOVA) followed by Student's *t* test in R software (ANOVA, $p < 2.2 \times 10^{-16}$, ***$p < 0.001$ compared to the free RFP). Scale bars: 300 μm.

which express GFP alone (Dai et al., 2020; Figure S8a,b). TuMV replication level was determined by RT-qPCR, using a TuMV-capsid primer pair (CP, Table 1) and normalized with the reference gene mCherry.

As shown in Figure S8b, none of the AtHVA22a mutants displayed a statistically significant reduced level of TuMV accumulation compared to WT in contrast to the negative control corresponding to

TABLE 1 Primers used in this study. Initiation codons are in blue and stop-codons are in red.

Primer name	Sequence (5′–3′)
Gateway	
pENT-6K2-Tup	CACCATGAACACCAGCGACATGAGC
pENT6K2-TumNOSTOP	TTCATGGGTTACGGGTTCGGACATC
pENT6K2-TumSTOP	CTATTCATGGGTTACGGGTTCGG
HVA22a_DTopoFwd	CACCATGGGATCTGGAGCTGGCAA
HVA22a_DtopoRevNostp	GTACTGATAACCCTCACCAT
HVA22a_DtopoRevStp	TTAGTACTGATAACCCTCACCAT
HVA22a_NterTMD_DTopoRevNostp	AGCAGCGCCACTAAAGTAGG
HVA22a_NterTMD_DTopoRevstp	TTAAGCAGCGCCACTAAAGTAGG
HVA22a_APHCter_DtopoFwd	CACCATGTATGTCTATGAACATTTTGT
HVA22a_M36 48 55_DTopoRevNostp	GCAGCTGTTAACACATCGTC
pENT-P3NPIPO-Tup	CACCATGGGAAAGAATGGGAGGAC
pENT-P3NPIPO-TumNOSTOP	CTACTCCGTTCGTAAGATGACATGAC
Reverse transcription-quantitative PCR	
qHVA22a2-Fwd	GCTGCTGAGAAGTACATTGC
qHVA22a2-Rev	ACCCTCACCATACATCGTTT
CP-F1	ATGTACCCAGGCTCAAGA GT
CP-R1	CGTTAGTTCGTAATCGGCCA
mCherry_Fwd1	ATGGTGAGCAAGGGCGAGGAGGAT
mCherry_Rev2	TCGCCCTCGCCCTCGATCTCGAACT
GFP-HDEL_Fwd	CTCGTCATGAGATCTGTATAG
GFP-HDEL_Rev	CCTGTCCTTTTACCAGAC
Ubiquitin_Fwd	CCTACCTTTGAGGGGCTTCT
Ubiquitin_Rev	GAAGTCGTGAGACAGCGTTG
Split-ubiquitin yeast two-hybrid	
HVA22a-Sfi1_Fwd	CGCAGAGTGGCCATTACGGCCATGGGATCTGGAGCTGGCAA
HVA22a-Sfi1_Rev	CTCGAGAGGCCGAGGCGGCCTTAGTACTGATAACCCTCACCAT
CRISPR-Cas9 mutants	
z5880-Fw (HVA22a guide RNA forward)	ACCCTCGGAGCATTAACATT
z5880-Rev (HVA22a guide RNA reverse)	AATGTTAATGCTCCGAGGGT
z6159-Fw (HVA22a targeted region)	CGAGCTCACATTCGCCAAAC
z6159-Rev (HVA22a targeted region)	CGGCCCATACAGTACACAAAA

At-KO-eIF(iso)4E mutant (Duprat et al., 2002), where TuMV accumulation was greatly reduced. To confirm those results, we conducted an alternative assessment of CP expression in function of GFP HDEL labelling using the TuMV-[W15A]6K2 mCherry//GFP-HDEL construct, still able to replicate but not able to move, that allows us to quantify only replication and not movement, as described in Rocher et al. (2022). The results shown in Figure S8c lead to the same conclusion: when normalized to the reference gene GFP-HDEL, CP expression did not vary in *Arabidopsis* mutants compared to the WT, whether the 6K2 is mutated or not. Therefore, using the non-moving TuMV-[W15A]6K2 mCherry virus that essentially recapitulates a protoplast experiment (where movement is prevented by separating the cells, but which otherwise has similar variability of initial viral dose), those results suggest that the truncation of the C-terminal cytoplasmic tail of AtHVA22a impacts TuMV cell-to-cell movement in the inoculated leaves but not drastically the level of replication.
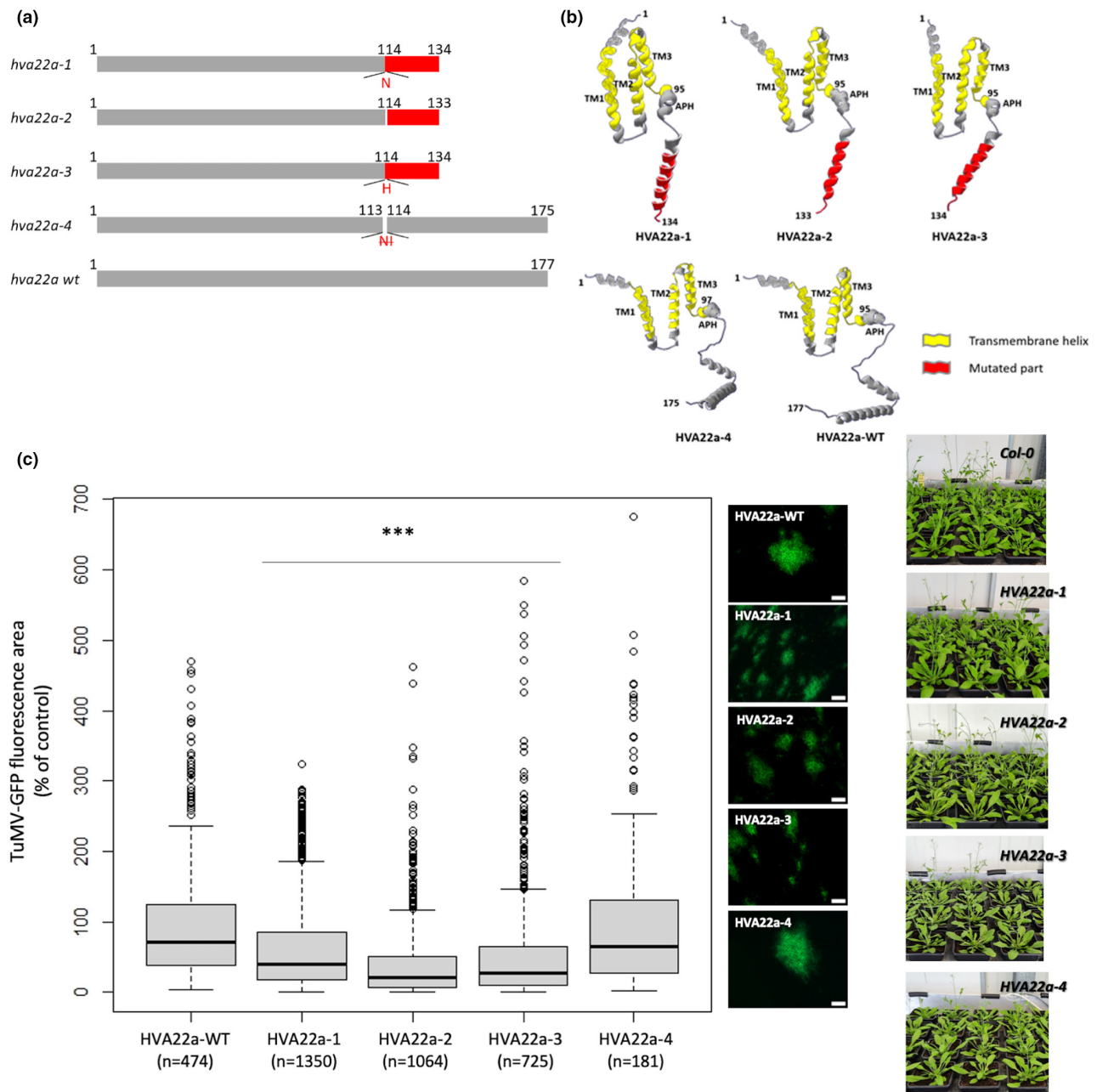
FIGURE 5 TuMV propagation is slowed down in three independent CRISPR-Cas9 mutants affected in the C-terminal cytosolic tail of AtHVA22a. (a) Schematic representation of the amino acid sequences of HVA22a mutants. In grey: wild-type (WT) sequence. In red, mutated sequence after a frameshift that induces premature stop codons in *hva22a-1*, *-2* and *-3* mutants. An extra asparagine (N) or histidine (H) is present at position 114 in hva22a-1 and hva22a-2 respectively. A deletion of amino acids N-113 and isoleucine (i)-114 occurs in *hva22a-4* mutant. The number of amino acids number is indicated for each protein at the C-terminus. (b) Alphafold 3D structure prediction of AtHVA22a and the CRISPR-Cas9 mutants. (c) The area of infection foci is normalized and expressed in % of the area of TuMV-GFP//mCherry propagation in WT plants. Between 181 and 1350 infection foci from at least three independent experiments were imaged at 5 days post-inoculation. Statistical analysis was performed using one-way analysis (ANOVA), followed by Student's *t* test in R software (ANOVA, $p < 2.2 \times 10^{-16}$; ***$p < 0.001$ compared to the WT). Scale bars: 300 μm.

3 | DISCUSSION

3.1 | Plant HVA22 proteins are involved in response to abiotic stresses

The first plant HVA22 was identified in barley aleurone cells (*H. vulgare*) as an abscisic acid (ABA)- and stress-induced protein (Shen et al., 1993, 2001). In barley vegetative tissues, the expression of *HVA22* was also shown to be induced by ABA, cold and drought. Since then, diverse abiotic stresses such as temperature, salinity and drought have been shown to differentially regulate the expression of HVA22 homologues in various plant species (Courtney et al., 2016; Gomes Ferreira et al., 2019; Lyu et al., 2021; Wai et al., 2022; Zhang, Wen, et al., 2023; Zhang, Yuan, et al., 2023). However, only

a limited number of studies describe the function of those HVA22 genes in plants. The expression of HVA22-GFP in aleurone cells in barley showed ER network and Golgi punctate fluorescence patterns, suggesting that HVA22 could participate in the ER-to-Golgi secretory pathway in planta (Guo & Ho, 2008). In *Arabidopsis*, Chen et al. (2009) showed that in RNAi transgenic lines where the expression levels of the four isoforms AtHVA22a, c, d and e were strongly reduced, autophagy activity was enhanced, suggesting a role of HVA22 homologues of a suppressor of autophagy.

3.2 | The role of plant HVA22 proteins in ER shaping is poorly documented

The ER appears as a polygonal network arrangement of interconnected tubules and cisternae stretching throughout the cytoplasm (Stefano et al., 2014). In animal and yeast, HVA22 homologues that are Reep/DP1/Yop1 family members, are responsible for the control of ER organization, together with proteins called reticulons. Reep/DP1/Yop1 proteins are ER-shaping proteins required to form an ER tubular network, probably by stabilizing the high curvature of the tubules (Hu et al., 2008; Park et al., 2010; Voeltz et al., 2006). However, a role for HVA22 proteins in plant ER integrity still remains very little documented. So far, only one plant HVA22 homologue has been shown to be involved in ER tubule formation. Meng et al. (2022) and Liang et al. (2023) showed that HVA22 rice homologue, OsHLP1, is localized at the ER, is a reticulum phagy receptor involved in ER homeostasis and positively regulates the immune response to *Magnaporthe oryzae*. In particular, the expression of OsHLP1-GFP in *N. benthamiana* cells and in rice protoplasts induced deformation of the ER tubule network. Such constriction of ER tubules is not observed during the transient expression of the two *Arabidopsis* homologues AtHVA22b (Lee et al., 2013) and AtHVA22d (Chen et al., 2011) in *Nicotiana tabacum* and *N. benthamiana* leaf epidermal cells, respectively. In the case of AtHVA22a homologue, here we showed that the transient expression of AtHVA22a-GFP or GFP-AtHVA22a did not induce any obvious ER deformation in *N. benthamiana* cells. GFP-HVA22a labelled the ER quite uniformly and it was also found at the nuclear envelope without apparent constriction of ER tubules, a similar pattern observed with overexpressed AtHVA22b (Lee et al., 2013). As there is no signal peptide in the AtHVA22a sequence, we could expect that fusing GFP at the N-terminus of the protein would interfere with a proper ER membrane insertion, but our results (Figure 2) showed the ER localization of AtHVA22a. However, we cannot exclude that the presence of the GFP tag could reduce/abolish a potential ER hyperconstriction or other still unknown function of AtHVA22a. However, for the barley protein, the HVA22-GFP fusion is able to perform similar functions as native HVA22 proteins in vivo (Guo & Ho, 2008): when compared with cells transformed with GFP, overexpression of HVA22-GFP also significantly reduced the percentage of vacuolated cells under control and gibberellic acid-treated conditions as the native protein in barley (Guo & Ho, 2008).

For the yeast homologue Yop1, His-tagged Yop1 protein does not induce tubules in vitro, even though it is able to form small vesicles similar to those formed by the non-tagged protein (Hu et al., 2008). So, it is possible that even though a small tag (6×His tag) is fused at the N-terminus of AtHVA22a, it still impairs ER constriction, although His and RFP fusions do not interfere with the effect on virus propagation as shown in Figure 4. Experiments performed with unfused AtHVA22a protein would allow us to answer this question, although, without available antibodies specifically targeting the AtHVA22a isoform, it remains difficult to confirm overexpression of unfused AtHVA22a. Therefore, we cannot conclude about a potential function of AtHVA22a in ER constriction in plants.

3.3 | AtHVA22a protein is the first HVA22 family member displaying some PD localization

AtHVA22a belongs to the proteins highly enriched in the PD proteome (Brault et al., 2019). As Reep/DP1/Yop1 proteins are involved in high curvature formation of ER membrane (Brands & Ho, 2002; Hu et al., 2008), one could hypothesize that AtHVA22a could be involved in the high curvature observed at the desmotubule ER at the level of PD. Tilsner et al. (2011) hypothesized that the degree of desmotubule constriction could indeed significantly affect SEL regulation. In our study, we observed some PD localization for AtHVA22a, confirming the proteomics data results, but PD colocalization was less obvious than expected for a PD-associated protein highly enriched in the PD proteome. However, we still cannot exclude that the GFP fusion may affect the subcellular localization of the protein, although, when co-expressed with the heterologous MP CMV 3a, a very clear PD localization was observed for AtHVA22a-GFP (Figure 2e), confirming that AtHVA22a can indeed be PD located. Furthermore, our results show that the ^{TuMV}6K2/AtHVA22a interaction signal observed in BiFC displays some proximity with the PD marker, which is not the case when the C-terminal domain of AtHVA22a is omitted, as the interacting signal remained associated to the ER network (Figure S3d). Furthermore, the ^{HVA22a}C-ter tail PD association was even increased during TuMV infection (Figure S3c), suggesting that the C-terminus domain of AtHVA22a is important for PD association of AtHVA22a. The C-terminal domain of AtHVA22a is truncated in the three CRISPR-Cas9 mutants *hva22a-1*, *-2* and *-3* leading to instability of the corresponding mutant proteins in *N. benthamiana*, in good agreement with Xiang et al. (2023) who also showed that the C-terminal part of Yop1 is critical for the stability and the function of the protein. So far, our subcellular observations of GFP fusions of the corresponding mutants did not allow us to observe a clear difference in PD colocalization between the mutants and the WT, even in infected condition (Figure S9). One hypothesis is that both C-terminally truncated proteins and ^{HVA22a}C-ter fragments might localize by interacting with native HVA22s present in PD as these the experiments were not done in a *KO* genetic background. Once again, without any available specific anti-AtHVA22a antibodies, we cannot check whether the CRISPR-Cas9 mutants display

also a lower accumulation of AtHVA22a. Whether PD permeability is altered in the three CRISPR-Cas9 mutants is currently under study. One must note that the phenotype of those mutants does not seem altered compared to WT, in contrast to transgenic AtHVA22d RNAi lines previously described that display slow growth rate, produce small siliques and have reduced seed yield (Chen et al., 2009). However, in those AtHVA22d-RNAi lines, the expression level of not only AtHVA22d, but also other homologues, AtHVA22a, c and e was lowered. In their study, the authors describe another transgenic AtHVA22a RNAi line where only the expression level of AtHVA22a is modified with a much weaker phenotype than the AtHVA22d-RNAi line, suggesting some functional redundancy between AtHVA22 homologues in *Arabidopsis*.

3.4 | AtHVA22a is involved in TuMV propagation and the C-terminal tail of the protein is important in this process

In our study, we showed that overexpression of AtHVA22a-RFP and -His-fusion favours the propagation of TuMV in *N. benthamiana*. Notably, although we controlled the subcellular pattern of RFP-fusion expression, in western blots we could observe some cleavage between the RFP tag and AtHVA22a (Figure S10 and Figure WB6), suggesting that in those experiments we cannot exclude that the effect observed was due to 'invisible' untagged AtHVA22a proteins beside the fusion RFP-HVA22a or HVA22a-RFP. Conversely, in CRISPR-Cas9 *Arabidopsis* mutants altered in the C-terminal cytoplasmic tail, the propagation of TuMV was slowed down in the three mutants with a truncated C-terminus (mutants *hva22a-1* to *-3*) whereas TuMV propagation in mutant *hva22a-4* (with two amino acids, in-frame deletion) was comparable to WT. Furthermore, our results showed that mutating the C-terminus of AtHVA22a did not impact drastically on the replication level of TuMV but could affect its cell-to-cell movement in the inoculated leaves.

3.5 | ^{TuMV}6K2 interacts with other proviral plant ER-shaping proteins, atlastin and reticulon-like proteins

Another protein involved in tubular ER shaping (ROOT HAIR DEFECTIVE3 or RHD3) has previously been shown to interact with ^{TuMV}6K2 (Movahed, Sun, et al., 2019). Atlastin-like GTPases of the RHD3 family are involved in membrane fusion and formation of three-way junctions in the polygonal network of ER tubules (Stefano et al., 2014; Sun & Zheng, 2018). In *Arabidopsis rhd3-8* mutant, both the replication and the intercellular movement of TuMV are impaired (Movahed, Sun, et al., 2019), and a role for RHD3 in the maturation of ^{TuMV}6K2-induced viral vesicles is suggested. However, as the effect of RHD3 inactivation on TuMV systemic infection is minor, the authors suggested that other fusion factors could be involved (Movahed, Sun, et al., 2019). It has also been reported that RHD3

is critical for the intercellular trafficking of the tomato spotted wilt tospovirus and its MP NSm (Feng et al., 2016). In this study, the authors suggested that, because NSm localized to both the ER and PD, the virus probably recruits essential host factors to facilitate its cell-to-cell movement via the desmotubule ER (Feng et al., 2016).

Remarkably, the plant RHD3 is the orthologue in yeast of the atlastin GTPase Sey1, that interacts with reticulons together with Yop1 (Lee et al., 2013). As ^{TuMV}6K2 interacts with RHD3 (Movahed, Sun, et al., 2019) and with AtHVA22a (this present study), AtHVA22a could also interact with RHD3, for the maturation of the 6K2-vesicles of TuMV. This is supported by our observations of a close proximity of the AtHVA22a/TuMV-6K2 interacting signal with 6K2-induced vesicles and the colocalization of AtHVA22a to the VRC during viral infection. No interaction between RHD3 and AtHVA22a has been described experimentally so far, but this interaction is strongly suggested by the interaction observed between their homologues in yeast (Faust et al., 2015; Lee et al., 2013). Interestingly, Chen et al. (2011) showed that the isoform AtHVA22d-YFP was not only localized to the tubular ER network but also was concentrated in punctae along the ER tubules, where it colocalized with a GFP-RHD3 fusion. Indeed, the authors frequently observed that those GFP-RHD3 punctae were often localized at the three-way junctions of tubules. Our own observations (Figure 1b) suggest that the punctae of AtHVA22a interacting with 6K2 could be indeed ER three-way junctions. Therefore, our results suggest that both RHD3 and AtHVA22a could both be involved together in TuMV 6K2-vesicles formation at the ER level.

Atlastins (homologues of RHD3) have also been shown to interact with reticulon proteins (RTNs) and DP1/YOP1 in animal and yeast cells (Lee et al., 2013). In *Arabidopsis*, reticulon proteins (called RTNLB) have also been described (Nziengui et al., 2007). The overexpression of a number of RTNLBs in tobacco leaf epidermal cells is sufficient to constrict the ER lumen and convert ER sheets into tubules (Sparkes et al., 2010; Tolley et al., 2008; Zhang, Wen, et al., 2023; Zhang, Yuan, et al., 2023), suggesting a conserved role for these proteins in eukaryotes. The membrane curvature is induced by two long hydrophobic regions displaying a wedge-like topology (Wang et al., 2021). In mammals and in yeast, RTNs have been shown to be proviral factors involved in viral infection (Aktepe et al., 2017; Diaz et al., 2010). For a plant RNA virus, brome mosaic virus (BMV, genus *Bromovirus*), in a yeast heterologous host system, Diaz et al. (2010) showed that reticulon homology proteins (RHPs) interact with protein 1a involved in replication, and that RHPs are directly involved in the formation and function of VRC. For the beet black scorch virus (BBSV, genus *Betanecrovirus*), the replication protein p23 is an ER-localized membrane protein that plays a key role in ER reorganization for the formation of ER-invaginated VRCs during BBSV infection (Cao et al., 2015). Very recently (Zhang, Wen, et al., 2023) demonstrated that RETICULON-LIKE PROTEIN B2 (NbRTNLB2) interacts with p23 of BBSV and that knocking down NbRTNLB2 expression in *N. benthamiana* inhibits BBSV replication and mitigates the p23-induced proliferation and aggregation of ER membranes. Whether knocking down NbRTNLB2 affects the formation of BBSV replication vesicles like that of BMV in yeast cells (Diaz et al., 2010) needs further investigation. NbRTNLB2

seems directly involved in the assembly of BBSV VRCs by inducing ER membrane rearrangements, a process requiring the presence of a functional APH domain in the C-terminus of the protein. In this study, by performing a proteomic analysis of biotinylated proteins enriched in p23-TurboID purification, besides RTNLB2, the authors also identified the homologue of AtHVA22a among the components of the p23-proximal proteome, together with other ER-associated factors, suggesting that NbHVA22a could also be involved in BBSV replication (Zhang, Wen, et al., 2023). Furthermore, the authors showed that [TuMV]6K2 protein and the viral replicase NIb both interact with NbRTNLB2 in BiFC experiments, and that the accumulation of TuMV is lowered in the inoculated leaves of NbRTNLB2-silenced *N. benthamiana* leaves at 3 dpi (Zhang, Wen, et al., 2023). Furthermore, as shown in Table S1, among the list of candidate genes obtained after SuY2H screening using 6K2 as a bait, we identified a homologue in *Arabidopsis* of NbRTNLB2 (AT4G11220). However, as this candidate was able to autoactivate the SuY2H system, we did not go further for functional validation. However, the results of Zhang, Wen, et al. (2023) strongly suggest that NbRTNLB2 is a reticulon protein that could play a role in replication of TuMV, although at this point it cannot be excluded that the reduction of the level of TuMV RNA in the silenced plants is also linked to a decrease in movement (Zhang, Wen, et al., 2023). Another protein with reticulon homology domain in soybean (GmRHP) was also shown to interact with the P3 protein of soybean mosaic potyvirus and to contribute to viral infection (Cui et al., 2018), confirming the involvement of reticulon-like proteins in potyvirus infection.

However, whether and how RTNs participate in viral replication and movement remains largely unexplored. It has been suggested that RTNs could be involved in PD regulation not only by actively constricting the desmotubule but also by bringing other proteins to membrane contact sites (Levy & Tilsner, 2020; Tilsner et al., 2011). Interestingly, some plant virus-encoded MPs mimic or interact with RTNs to facilitate viral movement (Lazareva et al., 2021; Tilsner & Kriechbaumer, 2022).

Whether interactions between HVA22 homologues and either RHD3 or RTN homologues occur in plants remains unknown. However, a member of the RTN family of *A. thaliana* (RTNLB13) was co-immunoprecipitated with the isoform of RHD3 (RHD3-like 2 [RL2]) suggesting that RTNs and RHD3 homologues can interact in planta (Lee et al., 2013).

3.6 | What are the mechanisms behind the positive effect of AtHVA22a on TuMV propagation?

Even though it appears clear that AtHVA22a could be involved in TuMV infection together with ER-shaping proteins such as RHD3 and reticulon-like proteins that both directly interact with [TuMV]6K2, a question remains: how can we explain that AtHVA22a interacts with 6K2 and is also colocalized at VRC, but only weakly at PD during TuMV infection, although we observe a slower TuMV propagation in the mutants affected in the C-terminal tail of AtHVA22a?

In order to quantify the level of accumulation of TuMV, independent of the movement, and as we did not succeed to efficiently transfect protoplasts isolated from leaves of WT and CRISPR-cCas9 mutants, we chose a remediating option to quantify TuMV accumulation relative to mCherry-HDEL or GFP-HDEL (a proxy for the number of initially infected cells), and showed that replication of TuMV is not drastically altered in the CRISPR-Cas9 mutants compared to WT. However, the surface of the infection foci observed in the three mutants *hva22a-1*, *-2* and *-3* was significantly smaller than in WT or *hva22a-4* mutant (where the C-terminal tail is not truncated). Therefore, either the lack of the C-terminal domain or the lower expression level and/or instability of the corresponding mutants, underlies the delayed movement of TuMV.

For potyviruses, both replication and movement (intra- and intercellular) are highly connected steps (Tilsner et al., 2013; Xue et al., 2023). As stressed by Movahed et al. (2017), the TuMV 6K2-induced vesicles are not only the site of viral replication, but also the vehicle for TuMV intercellular movement, and both CI and P3N-PIPO are involved in the intercellular movement of 6K2 vesicles. So, it is possible that the mutation of the C-terminal cytosolic tail of AtHVA22a would not affect the vesicle formation itself (as we observed that [HVA22a]TMD still interacts with 6K2 and at the VRC level), but would alter the 6K2-vesicle mobility towards the PD. Indeed, in yeast, a role of Yop1 in regulating vesicle trafficking has been suggested (Brands & Ho, 2002). In particular, vesicle budding has been speculated to benefit from the membrane curvature observed in ER tubules, as in yeast, most of the COPII vesicles, which transport cargo from the ER to Golgi, form in the tubular ER (Okamoto et al., 2012). Interestingly, the orthologous of AtHVA22k in *N. benthamiana*, was found in the list of factors co-immunoprecipitated with the 6K2 of the potyvirus potato virus A (PVA) during viral infection, suggesting that this AtHVA22k homologue could be part of the PVA VRC (Lõhmus et al., 2016). AtHVA22a could also be involved in the interactions between CI and P3N-PIPO and 6K2 that are crucial for TuMV intercellular movement (Movahed et al., 2017), or may also act directly in the constriction of the ER desmotubule and modifying the SEL of the PD.

Our present study shows that AtHVA22a protein represents a new proviral factor and we are only starting to identify the mechanisms behind its positive effect on TuMV propagation.

4 | EXPERIMENTAL PROCEDURES

4.1 | Plant materials, growth conditions, CRISPR-Cas9 mutants of AtHVA22a

Healthy and infected *N. benthamiana* and *A. thaliana* plants were maintained in a separate insect-proof greenhouse compartment (18/24°C night/day).

4.2 | AtHVA22a guide RNA cloning

To generate CRISPR-Cas9 mutants of AtHVA22a, a specific guide RNA (z5880, Table 1) targeting the *AtHVA22a* gene

(At1G74520) was designed using CRISPOR 4.7 (http://crispor.tefor.net/). Complementary nucleotides overhangs corresponding to the *Arabidopsis* U6 promoter (ATTG) and to the scaffold (AAAC) were added to the forward and reverse sequences of the guide RNA z5880 (ATTG + ACCCTCGGAGCATTAACATT and AAAC + AATGTTAATGCTCCGAGGGT, respectively). After the annealing of the forward and the reverse sequences, the resulting guide RNA sequence was inserted into the BsaI digested pTwist vector (Nadakuduti et al., 2019) containing a selectable marker gene *ntpII* and the resulting pTwist entry clone was verified by Sanger sequencing (Genoscreen, Lille) after plasmid DNA extraction using a miniprep kit (QIAGEN). The expression cassette of the *HVA22a* guide sequence was transferred by Gateway cloning (LR reaction) into a pDE-Cas9 destination vector containing spectinomycin resistance gene (for selection of bacterial clones after transformation) and a Basta resistance gene (for the selection of transformed *Arabidopsis* plants). The integrity of the guide RNA sequence cassette in the recombinant pDE-Cas9 vector was checked by sequencing (Genoscreen, Lille) before the transformation of *Agrobacterium tumefaciens* C58 with the recombinant pDE-Cas9 destination vector containing the HVA22a guide RNA sequence cassette.

4.3 | *Arabidopsis* Col-0 plant transformation

Agrobacteria transformed with the recombinant pDE-Cas9 vector were grown overnight at 28°C in Luria Bertani (LB) medium in presence of spectinomycin. Bacterial cells were pelleted by centrifugation (5000 rpm, 15 min, 4°C) and the pellet was resuspended in sucrose solution (10%) containing Silwet (0.05%) to reach an OD_{600} value of 0.9–1.2. This *Agrobacterium* suspension was used to transform 4-week-old *Arabidopsis* plants of Col-0 ecotype through the floral dip method (Clough & Bent, 1998).

4.4 | Plant selection and identification of HVA22a CRISPR-Cas9 mutants

Seeds of the transformed *Arabidopsis* Col-0 plants were sown on LB medium containing Basta (10 μg/mL) and 2-week-old T_1 seedlings that showed resistance and grew were transferred in soil. The plants were genotyped by PCR using specific primers pairs (z6159Fw and z6159Rev, Table 1) to detect potential mutations in the targeted region. Sanger sequencing of the 372 bp-length amplicons from 15 independent T_1 plants and analysis of the sequencing data using ICE Synthego (https://ice.synthego.com; Hsiau et al., 2018) allowed the identification of CRISPR-Cas9-edited plants. The transgenic plants were chosen for self-fertilization and their seeds were screened in T_2 generation to select *HVA22a* knockout lines. Screening of 72 T_2 generation plants allowed us to identify four *HVA22a* mutants with homozygous insertion or deletion (indels) (Figure S6).

4.5 | Molecular clones and fluorescent-tagged viral infectious clones

The cDNA of the candidate gene *AtHVA22a* was cloned from *A. thaliana* Col-0 library (used for SuY2H screening), the cDNAs corresponding to AtHVA22a-1 to -4 mutants, were cloned after extraction of total RNA from *A. thaliana* CRISPR-Cas9 mutants, and cDNA synthesis using the primers designed to amplify the full-length coding sequence (Table 1). All vector constructs were done following Gateway cloning strategies (www.lifetechnologies.com), using pENTR/DTOPO as entry vectors and pGWB-405/754/755 (Nakagawa et al., 2007) pSITE BiFC (Martin et al., 2009) as destination vectors. The cDNA of ^{TuMV}P3N-PIPO (Vijayapalani et al., 2012) ^{AtHVA22a}TMD (1–95 aa) and ^{AtHVA22a}C-ter (96–177 aa) were cloned in pENTR/DTOPO- vectors as entry vectors and pGWB-706 as destination vectors for subcellular localization experiments. The mCherry-PDCB1 (Plasmodesmata callose-binding protein 1), GFP-MCTP6 (Multiple C2 domains and transmembrane region protein) PD marker clones and BFP-HDEL (His-Asp-Glu-Leu) ER marker clones were kindly provided by Dr E. M. Bayer and were described in Brault et al. (2019). The pGreenTuMV/nGFP-cGUS (termed TuMV-GFP), pCambiaTuMV-6K2-mCherry (termed TuMV/6K2:mCherry), pCambiaTuMV/6K2:mCherry//GFP-HDEL, and the mutant pCambiaTuMV^{W15A}/6K2:mCherry//GFP-HDEL constructs were kindly supplied by Dr J. F Laliberté and described in Rocher et al. (2022). The pCBTuMV-GFP//mCherry-HDEL (termed TuMV-GFP//mCherry) clone was kindly provided by Dr A. Wang (Dai et al., 2020). For agroinoculation of the viral constructs in *N. benthamiana*, *A. tumefaciens* cells containing TuMV-derived clones were infiltrated into the leaves at an OD_{600} of 0.007. For *A. thaliana*, *A. tumefaciens* cells containing TuMV-derived clones were infiltrated via a specific buffer (10 mM MES pH 5.6, 10 mM $MgCl_2$, 150 μM acetosyringone) into the plant leaves at an OD_{600} between 0.5 and 0.6. To monitor TuMV-GFP propagation in the inoculated leaves, we optimized the OD values for agroinfiltration, in order to monitor at 5 dpi individual non-confluent infection foci (originating from single inoculated cells) under an AxioZoom microscope (Zeiss). The surface area of the infectious foci was measured using ImageJ software. As TuMV^{W15A}/6K2:mCherry mutant cannot move, it should be noted that a much higher OD for this mutant was used for agroinoculation compared to the WT, to get sufficient infected tissue for RT-qPCR analysis.

4.6 | Transient protein expression and confocal microscopy analyses

Agrobacterium tumefaciens cells harbouring the recombinant plasmids encoding fusion proteins were cultured at 28°C overnight to an OD_{600} of 0.8. For co-agroinfiltration and BiFC experiments, the *A. tumefaciens* suspensions were mixed in 1:1 ratio. In this mixture, the final dilution of the agrobacteria expressing each fusion protein was equivalent to an OD_{600} of 0.2 and the tombusviral silencing

suppressor protein P19 OD_{600} of 0.1 was added to enhance the transient expression in *N. benthamiana* cells (Jay et al., 2023). Agrobacteria mixtures were gently infiltrated with a 1 mL needle-free syringe in the lower epidermis of the leaves of 4-week-old *N. benthamiana*. Three to 5 days after agroinoculation, leaf samples were imaged using confocal LSM 880 microscopy (Zeiss) with a 20×, 40× or 63× oil immersion objectives to determine the subcellular localization of the overexpressed proteins. Aniline blue (25 µL/mL; Biosupplies) was infiltrated through the lower epidermal surface using a 1 mL needle-free syringe by gentle pressure, just before observation. The 405 nm diode laser was used to excite aniline blue or BFP-HDEL fluorochrome and emission light was captured between 463 nm and 491 nm. Argon and DPSS lasers were used to excite fluorescent proteins, and signals from both green and red channels were collected simultaneously. GFP and YFP were excited at 488 nm, and the emission light was captured at 499–544 nm; mCherry was excited at 561 nm, and the emission light was captured at 579–633 nm. Image processing was performed with ImageJ.

4.7 | Colocalization analysis using ImageJ software

The colocalization between the GFP-AtHVA22a signal and aniline blue labelling at the PD level was quantified using the centroid object-based method using the 3D objects counter plug-in of ImageJ software (Ito et al., 2021) as described in Rocher et al. (2022). The colocalized points number/total PD localized points number is the ratio of GFP-HVA22a PD localization. A statistical analysis was performed using the % of colocalization value for at least five images including at least 250 PD pit fields, using Kruskal–Wallis test.

The representative images of colocalization of GFP-HVA22a signal with aniline blue labelling at the PD level, or with BFP-HDEL labelling at ER level, were chosen to perform RGB profile plot in ImageJ's plug-in (https://imagej.net/plugins/rgb-profiler) to show the peaks of fluorescence intensities at different distances.

For other colocalization analysis the Coloc 2 in Fiji's plug-in (https://imagej.net/plugins/coloc-2) was used. The results of fluorescence colocalization studies can also be represented graphically in scatterplots where the intensity of one colour is plotted against the intensity of the second colour for each pixel. Under the conditions of proportional codistribution, the points of the scatterplot cluster around a straight line whose slope reflects the ratio of the fluorescence of the two probes. In contrast, the lack of colocalization is reflected by the distribution of points into two separate groups, each showing varying signal levels of one probe with little or no signal from the other probe (Dunn et al., 2011).

4.8 | RNA extraction and RT-qPCR

Total RNA extraction from *A. thaliana* WT and CRISPR-Cas9 mutant lines infected with TuMV-GFP//mCherry was performed using the NucleoSpin RNA Plant Kit (Macherey Nagel). Five independent plants for each condition were sampled in three independent experiments. The purified RNAs were treated once again by DNase I with the TURBO DNase-free kit (Invitrogen) and RNA concentration was determined by measuring absorbance at 230, 260 and 280 nm in a microplate UV–vis spectrophotometer (Agilent BioTek Instrument). The total RNA was adjusted to 50 mg/mL and was reverse transcribed according to the manufacturer's instructions using the RevertAid H-Minus enzyme (Thermo Scientific) and oligo(dT$_{18}$) primer. cDNA was used to perform the real-time quantitative PCR on the Light Cycler 480 Instrument II (Roche), using the Light Cycler 480 SYBR Green I MASTER Kit (Roche Diagnostics). The PCR mixture included per well 10 µL of master mix, 0.6 µL of each primer (0.3 mM) (*CP*, *mCherry* and *ubiquitin* as housekeeping gene; Table 1), 3.8 µL of water and 5 µL of cDNA. Thermal cycling conditions were as follows: 15 s at 95°C; followed by 40 cycles of 5 s at 95°C, 20 s at 58°C and 30 s at 72°C. The relative expression level of the target genes (*CP* and *mCherry*, fold-changes) was expressed according to the reference gene (*ubiquitin*) as $2^{-\Delta(Ct\ target\ gene-CtUb)}$. Then, ratios of *CP* on *mCherry* expression transcripts transcribed from the cassette of the same construct but independent of the TuMV virus were calculated in order to avoid the bias of agroinfiltration efficiency.

To quantify the expression level of AtHVA22a at 0 dpi and 6 dpi (inoculated leaves) and 13 dpi (systematically infected leaves), total RNA extraction from *A. thaliana* inoculated with GFP (mock condition) or infected with TuMV-GFP//mCherry was performed as described above. Four independent plants for each condition at the three time points were sampled in three independent experiments. RT-qPCR was performed as described above, using the primers qHVA22a2-Fwd and qHVA22a2-Rev (Table 1) that are specific to amplify the *AtHVA22a* copy. The relative expression level of the target gene, *AtHVA22a*, was expressed according to the reference gene (*ubiquitin*) as $2^{-\Delta(Ct\ target\ gene-CtUb)}$. The infection of TuMV in both inoculated leaves and systematically infected leaves was confirmed by RT-PCR with CP primers (Table 1).

4.9 | Interaction analyses through SuY2H and BiFC assays

Split ubiquitin analysis was performed using the Y2H system from DUALmembrane system (Dualsystems Biotech AG). AtHVA22a and ^{TuMV}6K2 cDNA were amplified by PCR using SfiI restriction site-containing primers (Table 1) with subsequent orientated cloning of cDNA into pPR3N prey and pBT3N bait vectors. The constructs pBT3N:CER1 and pPR3N:CytB5-B were kindly supplied by Bernard et al. (2012) and were used as an internal positive control as described in Rocher et al. (2022). THY.AP4 yeast strain (MATa *ura3 leu2 lexA-lacZ-TRP1 lexA-HIS3 lexA-ADE2*) cells were co-transformed with pBT3N:6K2 and pPR3N:HVA22a. The bait pBT3N:CER1 was used as a negative control for the prey pPR3N:HVA22a. The prey pPR3N:CytB5-B was used as a negative control for the bait

pBT3N:^{TuMV}6K2. Transformants were selected on medium lacking Trp and Leu (−TL), and interactions were assayed on stringent media lacking His, Trp and Leu (−HTL) and adenine (−AHTL) supplemented with 1 mM 3-AT (Sigma).

Protein–protein interactions were assessed in planta by BiFC as described in Rocher et al. (2022). ^{TuMV}6K2 cDNA was fused in-frame via the LR clonase Gateway reaction (Invitrogen) to the C-terminal half of YFP (NY) in the pSITE-nEYFP-C1 vector (ABRC CD3-1648) (i.e., nYFP-^{TuMV}6K2) and the cDNA encoding AtHVA22a to the N-terminal half of YFP (CY) in the pSITE-cEYFP-N1 vector (ABRC CD3-1651) (i.e., AtHVA22a-cYFP). pDONR HVA22a-TMD (1–97 aa) as entry vector (kindly supplied by Dr Jens Tilsner) was recombined with Destination vector pSITE-cEYFP-N1 vector (ABRC CD3-1651) (i.e., ^{AtHVA22a}TMD-cYFP). The cDNA encoding ^{AtHVA22a}C-ter (96–177 aa) was fused to the N-terminal half of YFP (CY) in the pSITE-cEYFP-N1 vector (ABRC CD3-1651) (i.e., ^{AtHVA22a}C-ter-cYFP). For fluorescence complementation tests, compatible combinations between protein pairs (i.e., providing both parts of the YFP) were assayed by transient expression following agroinfiltration of *N. benthamiana* leaves. YFP fluorescence was detected 3 days after infiltration by confocal fluorescence microscopy. The lambda scan mode confirmed that for some region-of-interest (ROI) spots, a maximum of fluorescence emission was observed at 530 nm, which corresponds to YFP emission wavelength.

4.10 | Protein analysis, western blots and quantitative western blots

Plant leaf tissue was ground in liquid nitrogen and 200 μL of the Laemmli buffer was added to the powder (200 mM Tris–HCl pH 6.8, 4% SDS, 20% glycerol, 0.05% bromophenol blue and 100 mM dithiothreitol). Following boiling for 10 min, the homogenate was centrifuged at 10,000 *g* for 1 min. Proteins were separated on 10% SDS-PAGE gels and blotted onto nitrocellulose membranes. The membranes were probed with antibodies raised against GFP (GFP rabbit polyclonal antibody, TP 401 AMSBIO, dilution 1:3000), antibodies raised against RFP (RFP mouse monoclonal antibodies, AS153028, Agrisera, dilution 1:3000), anti-polyhistidine monoclonal antibodies produced in mouse (H1029, Sigma, dilution 1:3000) or polyclonal antibodies recognizing the N- or C-terminal of YFP (Ref-AS11 1776 and Ref-AS11 1775 Agrisera, Vännas, Sweden, dilution 1:2000). Anti-rabbit IgGs coupled with peroxidase (A-9169 from Sigma-Aldrich, dilution 1:3000) or anti-mouse IgGs coupled with peroxidase (A-9044 from Sigma-Aldrich, dilution 1:3000) were used as secondary antibodies. Detection was finally achieved using the ChemiDoc Imaging System (Bio-Rad) and the Amersham ECL Western Blotting Detection Kit.

In quantitative western blots, proteins were separated in 10% TGX Stain-Free polyacrylamide gels at 300 V for 20–25 min. TGX Stain-Free polyacrylamide gels (10%) were mixed by acrylamide solutions and buffers from TGX Stain-Free FastCast Acrylamide Kit. In order to visualize the total proteins, the gels were then placed in a ChemiDoc MP Imaging System (Bio-Rad) for activation by exposure to UV light for 1 min. Proteins were transferred to a nitrocellulose membrane blot in 7 min using the Trans-Blot Turbo Transfer System (Bio-Rad). A stain-free blot image was taken using the ChemiDoc MP System for total protein measurement in each sample lane. Loading controls are two bands chosen from stain-free blot images. The blot was blocked in a blocking buffer (Rockland Immunochemicals, Inc.) for 1 h at room temperature and probed overnight at 4°C with primary antibody raised against GFP (GFP rabbit polyclonal antibody, TP 401 AMSBIO) or actin (actin rabbit, polyclonal antibody, AS13 2640 Agrisera, dilution 1:5000). Horseradish peroxidase (HRP)-conjugated goat anti-rabbit antibodies (Sigma-Aldrich) applied to the blot at a dilution of 1:3000 for 1 h at room temperature. All antibodies were diluted in blocking buffer. Chemiluminescent signals were developed using Clarity Western ECL substrate (Bio-Rad) and captured by the ChemiDoc MP System. Image data were analysed using Image Lab v. 4.1 Software (Bio-Rad). Statistical analysis was done using Microsoft Excel Software.

4.11 | In silico analysis and statistical analysis

Statistical analysis was performed using R v. 4.2.2 software. As mentioned in the figure legends, statistical significance was determined using either a Kruskal–Wallis bilateral test for GFP-HVA22a PD localization or a one-way analysis of variance, when significant ($p < 0.05$), followed by a Student's *t* test for the other experiments. The protein 3D structure predictions were performed by using AlphaFold in google colab website (https://colab.research.google.com/github/deepmind/alphafold/blob/main/notebooks/AlphaFold.ipynb) and edited by using SPDBV_4.10 (Jumper et al., 2021). The predictions of transmembrane domains were performed by using Phyre2 website (http://www.sbg.bio.ic.ac.uk/~phyre2/html/page.cgi?id=index; Kelley et al., 2015). Alignments were performed using ClustalW (https://www.genome.jp/tools-bin/clustalw; Thompson et al., 1994). The website 'Easy Sequencing in PostScript' (ESPript) was used to render sequence similarities and secondary structure information from aligned sequences (https://espript.ibcp.fr/ESPript/ESPript/index.php; Robert & Gouet, 2014).

4.12 | Construction of phylogenetic tree

The amino acids sequences of *A. thaliana* HVA22 used for phylogenetic analysis were downloaded from the website TAIR (https://www.arabidopsis.org/). The phylogenetic tree was constructed by using maximum-likelihood method and the best protein model (LG+G+I+F) was chosen according to the Model Analysis in MEGA 11 (Tamura et al., 2021).

DATA AVAILABILITY STATEMENT

The datasets used and/or analysed during the current study are available from the corresponding author on reasonable request. Sequence data is available at GenBank at https://www.ncbi.nlm.nih.gov/genbank/ with accession numbers: At1G74520 (AtHVA22a); At5G62490 (AtHVA22b); At1G69700 (AtHVA22c); At4G24960 (AtHVA22d); At5G50720 (AtHVA22e); At2G42820 (AtHVA22f); AT1G75700 (AtHVA22g); AT1G19950 (AtHVA22h); AT5G42560 (AtHAV22i); AT2G36020 (AtHVA22j); AT4G36720 (AtHVA22k); NC_002509.2[5744..5902] (TuMV6K2).

ORCID

Jean-Luc Gallois 🆔 https://orcid.org/0000-0003-0451-1740
Sylvie German-Retana 🆔 https://orcid.org/0000-0002-8702-2856

REFERENCES

Aktepe, T.E., Liebscher, S., Prier, J.E., Simmons, C.P. & Mackenzie, J.M. (2017) The host protein reticulon 3.1A is utilized by flaviviruses to facilitate membrane remodelling. *Cell Reports*, 21, 1639–1654.

Angelotti, T. (2022) Exploring the eukaryotic yip and REEP/Yop superfamily of membrane-shaping adapter proteins (MSAPs): a cacophony or harmony of structure and function? *Frontiers in Molecular Biosciences*, 9, 912848.

Beauchemin, C. & Laliberté, J.-F. (2007) The poly(a) binding protein is internalized in virus-induced vesicles or redistributed to the nucleolus during turnip mosaic virus infection. *Journal of Virology*, 81, 10905–10913.

Benitez-Alfonso, Y., Faulkner, C., Ritzenthaler, C. & Maule, A.J. (2010) Plasmodesmata: gateways to local and systemic virus infection. *Molecular Plant–Microbe Interactions*, 23, 1403–1412.

Bernard, A., Domergue, F., Pascal, S., Jetter, R., Renne, C., Faure, J.-D. et al. (2012) Reconstitution of plant alkane biosynthesis in yeast demonstrates that *Arabidopsis* ECERIFERUM1 and ECERIFERUM3 are core components of a very-long-chain alkane synthesis complex. *The Plant Cell*, 24, 3106–3118.

Brady, J.P., Claridge, J.K., Smith, P.G. & Schnell, J.R. (2015) A conserved amphipathic helix is required for membrane tubule formation by Yop1p. *Proceedings of the National Academy of Sciences of the United States of America*, 112, E639–E648.

Brands, A. & Ho, T.D. (2002) Function of a plant stress-induced gene, *HVA22*. Synthetic enhancement screen with its yeast homolog reveals its role in vesicular traffic. *Plant Physiology*, 130, 1121–1131.

Brault, M.L., Petit, J.D., Immel, F., Nicolas, W.J., Glavier, M., Brocard, L. et al. (2019) Multiple C2 domains and transmembrane region proteins (MCTPs) tether membranes at plasmodesmata. *EMBO Reports*, 20, e47182.

Cabanillas, D.G., Jiang, J., Movahed, N., Germain, H., Yamaji, Y., Zheng, H. et al. (2018) Turnip mosaic virus uses the SNARE protein VTI11 in an unconventional route for replication vesicle trafficking. *The Plant Cell*, 30, 2594–2615.

Cao, X., Jin, X., Zhang, X., Li, Y., Wang, C., Wang, X. et al. (2015) Morphogenesis of endoplasmic reticulum membrane-invaginated vesicles during beet black scorch virus infection: role of auxiliary replication protein and new implications of three-dimensional architecture. *Journal of Virology*, 89, 6184–6195.

Chen, C.-N., Chu, C.-C., Zentella, R., Pan, S.-M. & David, T.-H. (2002) *AtHVA22* gene family in *Arabidopsis*: phylogenetic relationship, ABA and stress regulation, and tissue-specific expression. *Plant Molecular Biology*, 49, 631–642.

Chen, C.-N.N., Chen, H.-R., Yeh, S.-Y., Vittore, G. & Ho, T.-H.D. (2009) Autophagy is enhanced and floral development is impaired in *AtHVA22d* RNA interference *Arabidopsis*. *Plant Physiology*, 149, 1679–1689.

Chen, J., Stefano, G., Brandizzi, F. & Zheng, H. (2011) *Arabidopsis* RHD3 mediates the generation of the tubular ER network and is required for Golgi distribution and motility in plant cells. *Journal of Cell Science*, 124, 2241–2252.

Cheng, G., Dong, M., Xu, Q., Peng, L., Yang, Z., Wei, T. et al. (2017) Dissecting the molecular mechanism of the subcellular localization and cell-to-cell movement of the sugarcane mosaic virus P3N-PIPO. *Scientific Reports*, 7, 9868.

Chung, B.Y., Miller, W.A., Atkins, J.F. & Firth, A.E. (2008) An overlapping essential gene in the *Potyviridae*. *Proceedings of the National Academy of Sciences of the United States of America*, 105, 5897–5902.

Clough, S.J. & Bent, A.F. (1998) Floral dip: a simplified method for *Agrobacterium*-mediated transformation of *Arabidopsis thaliana*. *The Plant Journal*, 16, 735–743.

Courtney, A.J., Xu, J. & Xu, Y. (2016) Responses of growth, antioxidants and gene expression in smooth cordgrass (*Spartina alterniflora*) to various levels of salinity. *Plant Physiology and Biochemistry*, 99, 162–170.

Cronin, S., Verchot, J., Haldeman-Cahill, R., Schaad, M.C. & Carrington, J.C. (1995) Long-distance movement factor: a transport function of the potyvirus helper component proteinase. *The Plant Cell*, 7, 549–559.

Cui, H. & Wang, A. (2016) Plum pox virus 6K1 protein is required for viral replication and targets the viral replication complex at the early stage of infection. *Journal of Virology*, 90, 5119–5131.

Cui, X., Lu, L., Wang, Y., Yuan, X. & Chen, X. (2018) The interaction of soybean reticulon homology domain protein (GmRHP) with *Soybean mosaic virus* encoded P3 contributes to the viral infection. *Biochemical and Biophysical Research Communications*, 495, 2105–2110.

Cui, X., Wei, T., Chowda-Reddy, R.V., Sun, G. & Wang, A. (2010) The *tobacco etch virus* P3 protein forms mobile inclusions via the early secretory pathway and traffics along Actin microfilaments. *Virology*, 397, 56–63.

Cui, X., Yaghmaian, H., Wu, G., Wu, X., Chen, X., Thorn, G. et al. (2017) The C-terminal region of the Turnip mosaic virus P3 protein is essential for viral infection via targeting P3 to the viral replication complex. *Virology*, 510, 147–155.

Dai, Z., He, R., Bernards, M.A. & Wang, A. (2020) The *cis*-expression of the coat protein of turnip mosaic virus is essential for viral intercellular movement in plants. *Molecular Plant Pathology*, 21, 1194–1211.

Deng, P., Wu, Z. & Wang, A. (2015) The multifunctional protein CI of potyviruses plays interlinked and distinct roles in viral genome replication and intercellular movement. *Virology Journal*, 12, 141.

Diaz, A., Wang, X. & Ahlquist, P. (2010) Membrane-shaping host reticulon proteins play crucial roles in viral RNA replication compartment formation and function. *Proceedings of the National Academy of Sciences of the United States of America*, 107, 16291–16296.

Dufresne, P.J., Thivierge, K., Cotton, S., Beauchemin, C., Ide, C., Ubalijoro, E. et al. (2008) Heat shock 70 protein interaction with *Turnip mosaic virus* RNA-dependent RNA polymerase within virus-induced membrane vesicles. *Virology*, 374, 217–227.

Dunn, K.W., Kamocka, M.M. & McDonald, J.H. (2011) A practical guide to evaluating colocalization in biological microscopy. *American Journal of Physiology—Cell Physiology*, 300, C723–C742.

Duprat, A., Caranta, C., Revers, F., Menand, B., Browning, K.S. & Robaglia, C. (2002) The *Arabidopsis* eukaryotic initiation factor (iso)4E is dispensable for plant growth but required for susceptibility to potyviruses. *The Plant Journal*, 32, 927–934.

Fan, S., Liu, H. & Li, L. (2022) The REEP family of proteins: molecular targets and role in pathophysiology. *Pharmacological Research*, 185, 106477.

Faust, J.E., Desai, T., Verma, A., Ulengin, I., Sun, T.-L., Moss, T.J. et al. (2015) The Atlastin C-terminal tail is an amphipathic helix that perturbs the bilayer structure during endoplasmic reticulum homotypic fusion. *Journal of Biological Chemistry*, 290, 4772–4783.

Felsenstein, J. (1985) Confidence limits on phylogenies: an approach using the bootstrap. *Evolution*, 39, 783–791.

Feng, Z., Xue, F., Xu, M., Chen, X., Zhao, W., Garcia-Murria, M.J. et al. (2016) The ER-membrane transport system is critical for intercellular trafficking of the NSm movement protein and tomato spotted wilt tospovirus. *PLoS Pathogens*, 12, e1005443.

Geng, C., Cong, Q.-Q., Li, X.-D., Mou, A.-L., Gao, R., Liu, J.-L. et al. (2015) Developmentally regulated plasma membrane protein of *Nicotiana benthamiana* contributes to potyvirus movement and transports to plasmodesmata via the early secretory pathway and the actomyosin system. *Plant Physiology*, 167, 394–410.

German, L., Yeshvekar, R. & Benitez-Alfonso, Y. (2023) Callose metabolism and the regulation of cell walls and plasmodesmata during plant mutualistic and pathogenic interactions. *Plant, Cell & Environment*, 46, 391–404.

Gomes Ferreira, M.D., Araújo Castro, J., Santana Silva, R.J. & Micheli, F. (2019) HVA22 from citrus: a small gene family whose some members are involved in plant response to abiotic stress. *Plant Physiology and Biochemistry*, 142, 395–404.

González, R., Wu, B., Li, X., Martínez, F. & Elena, S.F. (2019) Mutagenesis scanning uncovers evolutionary constraints on tobacco etch potyvirus membrane-associated 6K2 protein. *Genome Biology and Evolution*, 11, 1207–1222.

Grangeon, R., Agbeci, M., Chen, J., Grondin, G., Zheng, H. & Laliberte, J.-F. (2012) Impact on the endoplasmic reticulum and Golgi apparatus of turnip mosaic virus infection. *Journal of Virology*, 86, 9255–9265.

Grangeon, R., Jiang, J., Wan, J., Agbeci, M., Zheng, H. & Laliberté, J.-F. (2013) 6K2-induced vesicles can move cell to cell during turnip mosaic virus infection. *Frontiers in Microbiology*, 4, 351.

Grison, M.S., Brocard, L., Fouillen, L., Nicolas, W., Wewer, V., Dörmann, P. et al. (2015) Specific membrane lipid composition is important for plasmodesmata function in *Arabidopsis*. *The Plant Cell*, 27, 1228–1250.

Guo, W.-J. & Ho, T.-H. (2008) An abscisic acid-induced protein, HVA22, inhibits gibberellin-mediated programmed cell death in cereal aleurone cells. *Plant Physiology*, 147, 1710–1722.

Gutiérrez, S., Pirolles, E., Yvon, M., Baecker, V., Michalakis, Y. & Blanc, S. (2015) The multiplicity of cellular infection changes depending on the route of cell infection in a plant virus. *Journal of Virology*, 89, 9665–9675.

Heinlein, M. (2015) Plasmodesmata: channels for viruses on the move. *Methods in Molecular Biology*, 1217, 25–52.

Hsiau, T., Maures, T., Waite, K., Yang, J., Kelso, R., Holden, K. et al. (2018) Inference of CRISPR edits from Sanger trace data. *bioRxiv*, 251082. [Preprint].

Hu, J., Shibata, Y., Voss, C., Shemesh, T., Li, Z., Coughlin, M. et al. (2008) Membrane proteins of the endoplasmic reticulum induce high-curvature tubules. *Science*, 319, 1247–1250.

Inoue-Nagata, A.K., Jordan, R., Kreuze, J., Li, F., López-Moya, J.J., Mäkinen, K. et al. (2022) ICTV Virus Taxonomy Profile: *Potyviridae* 2022. *Journal of General Virology*, 103, Article 1738. Available from: https://doi.org/10.1099/jgv.0.001738

Ito, Y., Esnay, N., Platre, M.P., Wattelet-Boyer, V., Noack, L.C., Fougère, L. et al. (2021) Sphingolipids mediate polar sorting of PIN2 through phosphoinositide consumption at the trans-Golgi network. *Nature Communications*, 12, 4267.

Jay, F., Brioudes, F. & Voinnet, O. (2023) A contemporary reassessment of the enhanced transient expression system based on the tombusviral silencing suppressor protein P19. *The Plant Journal*, 113, 186–204.

Jiang, J., Patarroyo, C., Garcia Cabanillas, D., Zheng, H. & Laliberté, J.-F. (2015) The vesicle-forming $6K_2$ protein of turnip mosaic virus interacts with the COPII Coatomer Sec24a for viral systemic infection. *Journal of Virology*, 89, 6695–6710.

Jumper, J., Evans, R., Pritzel, A., Green, T., Figurnov, M., Ronneberger, O. et al. (2021) Highly accurate protein structure prediction with AlphaFold. *Nature*, 596, 583–589.

Kelley, L.A., Mezulis, S., Yates, C.M., Wass, M.N. & Sternberg, M.J.E. (2015) The Phyre2 web portal for protein modeling, prediction and analysis. *Nature Protocols*, 10, 845–858.

Klein, P.G., Klein, R.R., Rodriguez-Cerezo, E., Hunt, A.G. & Shaw, J.G. (1994) Mutational analysis of the tobacco vein mottling virus genome. *Virology*, 204, 759–769.

Kumar, G. & Dasgupta, I. (2021) Variability, functions and interactions of plant virus movement proteins: what do we know so far? *Microorganisms*, 9, 695.

Lazareva, E.A., Lezzhov, A.A., Chergintsev, D.A., Golyshev, S.A., Dolja, V.V., Morozov, S.Y. et al. (2021) Reticulon-like properties of a plant virus-encoded movement protein. *New Phytologist*, 229, 1052–1066.

Le, S.Q. & Gascuel, O. (2008) An improved general amino acid replacement matrix. *Molecular Biology and Evolution*, 25, 1307–1320.

Lee, H., Sparkes, I., Gattolin, S., Dzimitrowicz, N., Roberts, L.M., Hawes, C. et al. (2013) An *Arabidopsis* reticulon and the atlastin homologue *RHD3-like2* act together in shaping the tubular endoplasmic reticulum. *New Phytologist*, 197, 481–489.

Levy, A. & Tilsner, J. (2020) Creating contacts between replication and movement at plasmodesmata—a role for membrane contact sites in plant virus infections? *Frontiers in Plant Science*, 11, 862.

Liang, Y., Meng, F., Zhao, X., He, X. & Liu, J. (2023) OsHLP1 is an endoplasmic-reticulum-phagy receptor in rice plants. *Cell Reports*, 26, 113480.

Lõhmus, A., Varjosalo, M. & Mäkinen, K. (2016) Protein composition of 6K2-induced membrane structures formed during *Potato virus A* infection: PVA replication complex proteome. *Molecular Plant Pathology*, 17, 943–958.

Lyu, J.I., Ramekar, R., Kim, J.M., Hung, N.N., Seo, J.S., Kim, J.-B. et al. (2021) Unraveling the complexity of faba bean (*Vicia faba* L.) transcriptome to reveal cold-stress-responsive genes using long-read isoform sequencing technology. *Scientific Reports*, 11, 21094.

Martin, K., Kopperud, K., Chakrabarty, R., Banerjee, R., Brooks, R. & Goodin, M.M. (2009) Transient expression in *Nicotiana benthamiana* fluorescent marker lines provides enhanced definition of protein localization, movement and interactions *in planta*. *The Plant Journal*, 59, 150–162.

Martínez-Turiño, S. & García, J.A. (2020) Potyviral coat protein and genomic RNA: a striking partnership leading virion assembly and more. *Advances in Virus Research*, 108, 165–211.

Meng, F., Zhao, Q., Zhao, X., Yang, C., Liu, R., Pang, J. et al. (2022) A rice protein modulates endoplasmic reticulum homeostasis and coordinates with a transcription factor to initiate blast disease resistance. *Cell Reports*, 39, 110941.

Miyashita, S. & Kishino, H. (2010) Estimation of the size of genetic bottlenecks in cell-to-cell movement of soil-borne wheat mosaic virus and the possible role of the bottlenecks in speeding up selection of variations in *trans*-acting genes or elements. *Journal of Virology*, 84, 1828–1837.

Monsion, B., Froissart, R., Michalakis, Y. & Blanc, S. (2008) Large bottleneck size in cauliflower mosaic virus populations during host plant colonization. *PLoS Pathogens*, 4, e1000174.

Movahed, N., Cabanillas, D.G., Wan, J., Vali, H., Laliberté, J.-F. & Zheng, H. (2019) Turnip mosaic virus components are released into the extracellular space by vesicles in infected leaves. *Plant Physiology*, 180, 1375–1388.

Movahed, N., Patarroyo, C., Sun, J., Vali, H., Laliberté, J.-F. & Zheng, H. (2017) Cylindrical inclusion protein of turnip mosaic virus serves as a docking point for the intercellular movement of viral replication vesicles. *Plant Physiology*, 175, 1732–1744.

Movahed, N., Sun, J., Vali, H., Laliberté, J.-F. & Zheng, H. (2019) A host ER fusogen is recruited by *Turnip mosaic virus* for maturation of viral replication vesicles. *Plant Physiology*, 179, 507–518.

Nadakuduti, S.S., Starker, C.G., Voytas, D.F., Buell, C.R. & Douches, D.S. (2019) Genome editing in potato with CRISPR/Cas9. *Methods in Molecular Biology*, 1917, 183–201.

Nakagawa, T., Suzuki, T., Murata, S., Nakamura, S., Hino, T., Maeo, K. et al. (2007) Improved gateway binary vectors: high-performance vectors for creation of fusion constructs in transgenic analysis of plants. *Bioscience Biotechnology and Biochemistry*, 71, 2095–2100.

Nziengui, H., Bouhidel, K., Pillon, D., Der, C., Marty, F. & Schoefs, B. (2007) Reticulon-like proteins in *Arabidopsis thaliana*: structural organization and ER localization. *FEBS Letters*, 581, 3356–3362.

Okamoto, M., Kurokawa, K., Matsuura-Tokita, K., Saito, C., Hirata, R. & Nakano, A. (2012) High-curvature domains of the ER are important for the organization of ER exit sites in *Saccharomyces cerevisiae*. *Journal of Cell Science*, 125, 3412–3420.

Park, S.-H., Li, F., Renaud, J., Shen, W., Li, Y., Guo, L. et al. (2017) NbEXPA1, an α-expansin, is plasmodesmata-specific and a novel host factor for potyviral infection. *The Plant Journal*, 92, 846–861.

Park, S.H., Zhu, P.-P., Parker, R.L. & Blackstone, C. (2010) Hereditary spastic paraplegia proteins REEP1, spastin, and atlastin-1 coordinate microtubule interactions with the tubular ER network. *Journal of Clinical Investigation*, 120, 1097–1110.

Quenouille, J., Montarry, J., Palloix, A. & Moury, B. (2013) Farther, slower, stronger: how the plant genetic background protects a major resistance gene from breakdown: mechanisms of polygenic resistance durability. *Molecular Plant Pathology*, 14, 109–118.

Reagan, B.C. & Burch-Smith, T.M. (2020) Viruses reveal the secrets of plasmodesmal cell biology. *Molecular Plant–Microbe Interactions*, 33, 26–39.

Revers, F. & García, J.A. (2015) Molecular biology of potyviruses. *Advances in Virus Research*, 92, 101–199.

Robert, X. & Gouet, P. (2014) Deciphering key features in protein structures with the new ENDscript server. *Nucleic Acids Research*, 42, W320–W324.

Rocher, M., Simon, V., Jolivet, M.-D., Sofer, L., Deroubaix, A.-F., Germain, V. et al. (2022) StREM1.3 REMORIN protein plays an agonistic role in potyvirus cell-to-cell movement *in N. benthamiana. Viruses*, 14, 574.

Salmon, M.S. & Bayer, E.M.F. (2013) Dissecting plasmodesmata molecular composition by mass spectrometry-based proteomics. *Frontiers in Plant Science*, 3, 307.

Schoelz, J.E., Harries, P.A. & Nelson, R.S. (2011) Intracellular transport of plant viruses: finding the door out of the cell. *Molecular Plant*, 4, 813–831.

Shen, Q., Chen, C.-N., Brands, A., Pan, S.-M. & Ho, T.-H.D. (2001) The stress- and abscisic acid-induced barley gene *HVA22*: developmental regulation and homologues in diverse organisms. *Plant Molecular Biology*, 45, 327–340.

Shen, Q., Uknes, S.J. & Ho, T.H. (1993) Hormone response complex in a novel abscisic acid and cycloheximide-inducible barley gene. *Journal of Biological Chemistry*, 268, 23652–23660.

Simpson, C., Thomas, C., Findlay, K., Bayer, E. & Maule, A.J. (2009) An *Arabidopsis* GPI-anchor plasmodesmal neck protein with callose binding activity and potential to regulate cell-to-cell trafficking. *The Plant Cell*, 21, 581–594.

Solovyev, A.G., Atabekova, A.K., Lezzhov, A.A., Solovieva, A.D., Chergintsev, D.A. & Morozov, S.Y. (2022) Distinct mechanisms of endomembrane reorganization determine dissimilar transport pathways in plant RNA viruses. *Plants*, 11, 2403.

Sorel, M., Garcia, J.A. & German-Retana, S. (2014) The *Potyviridae* cylindrical inclusion helicase: a key multipartner and multifunctional protein. *Molecular Plant–Microbe Interactions*, 27, 215–226.

Sparkes, I., Tolley, N., Aller, I., Svozil, J., Osterrieder, A., Botchway, S. et al. (2010) Five *Arabidopsis* reticulon isoforms share endoplasmic reticulum location, topology, and membrane-shaping properties. *The Plant Cell*, 22, 1333–1343.

Stefano, G., Hawes, C. & Brandizzi, F. (2014) ER—the key to the highway. *Current Opinion in Plant Biology*, 22, 30–38.

Sun, J. & Zheng, H. (2018) Efficient ER fusion requires a dimerization and a C-terminal tail mediated membrane anchoring of RHD3. *Plant Physiology*, 176, 406–417.

Tamura, K., Stecher, G. & Kumar, S. (2021) MEGA11: molecular evolutionary genetics analysis version 11. *Molecular Biology and Evolution*, 38, 3022–3027.

Thivierge, K., Cotton, S., Dufresne, P.J., Mathieu, I., Beauchemin, C., Ide, C. et al. (2008) Eukaryotic elongation factor 1A interacts with *Turnip mosaic virus* RNA-dependent RNA polymerase and VPg-Pro in virus-induced vesicles. *Virology*, 377, 216–225.

Thompson, J.D., Higgins, D.G. & Gibson, T.J. (1994) CLUSTAL W: improving the sensitivity of progressive multiple sequence alignment through sequence weighting, positions-specific gap penalties and weight matrix choice. *Nucleic Acids Research*, 22, 4673–4680.

Tilsner, J., Amari, K. & Torrance, L. (2011) Plasmodesmata viewed as specialised membrane adhesion sites. *Protoplasma*, 248, 39–60.

Tilsner, J. & Kriechbaumer, V. (2022) Reticulons 3 and 6 interact with viral movement proteins. *Molecular Plant Pathology*, 23, 1807–1814.

Tilsner, J., Linnik, O., Louveaux, M., Roberts, I.M., Chapman, S.N. & Oparka, K.J. (2013) Replication and trafficking of a plant virus are coupled at the entrances of plasmodesmata. *Journal of Cell Biology*, 201, 981–995.

Tolley, N., Sparkes, I.A., Hunter, P.R., Craddock, C.P., Nuttall, J., Roberts, L.M. et al. (2008) Overexpression of a plant reticulon remodels the lumen of the cortical endoplasmic reticulum but does not perturb protein transport. *Traffic*, 9, 94–102.

Uchiyama, A., Shimada-Beltran, H., Levy, A., Zheng, J.Y., Javia, P.A. & Lazarowitz, S.G. (2014) The *Arabidopsis* synaptotagmin SYTA regulates the cell-to-cell movement of diverse plant viruses. *Frontiers in Plant Science*, 5, 584.

Vijayapalani, P., Maeshima, M., Nagasaki-Takekuchi, N. & Miller, W.A. (2012) Interaction of the trans-frame potyvirus protein P3N-PIPO with host protein PCaP1 facilitates potyvirus movement. *PLoS Pathogens*, 8, e1002639.

Voeltz, G.K., Prinz, W.A., Shibata, Y., Rist, J.M. & Rapoport, T.A. (2006) A class of membrane proteins shaping the tubular endoplasmic reticulum. *Cell*, 124, 573–586.

Wai, A.H., Waseem, M., Cho, L.-H., Kim, S.-T., Lee, D., Kim, C.-K. et al. (2022) Comprehensive genome-wide analysis and expression pattern profiling of the *SlHVA22* gene family unravels their likely

involvement in the abiotic stress adaptation of tomato. *International Journal of Molecular Sciences*, 23, 12222.

Wan, J. & Laliberté, J.-F. (2015) Membrane-associated virus replication complexes locate to plant conducting tubes. *Plant Signaling & Behavior*, 10, e1042639.

Wang, A. (2021) Cell-to-cell movement of plant viruses via plasmodesmata: a current perspective on potyviruses. *Current Opinion in Virology*, 48, 10–16.

Wang, N., Clark, L.D., Gao, Y., Kozlov, M.M., Shemesh, T. & Rapoport, T.A. (2021) Mechanism of membrane-curvature generation by ER-tubule shaping proteins. *Nature Communications*, 12, 568.

Wei, T., Huang, T.-S., McNeil, J., Laliberté, J.-F., Hong, J., Nelson, R.S. et al. (2010) Sequential recruitment of the endoplasmic reticulum and chloroplasts for plant potyvirus replication. *Journal of Virology*, 84, 799–809.

Wei, T., Zhang, C., Hong, J., Xiong, R., Kasschau, K.D., Zhou, X. et al. (2010) Formation of complexes at plasmodesmata for potyvirus intercellular movement is mediated by the viral protein P3N-PIPO. *PLoS Pathogens*, 6, e1000962.

Wen, R.H. & Hajimorad, M.R. (2010) Mutational analysis of the putative pipo of soybean mosaic virus suggests disruption of PIPO protein impedes movement. *Virology*, 400, 1–7.

Wu, G., Cui, X., Dai, Z., He, R., Li, Y., Yu, K. et al. (2020) A plant RNA virus hijacks endocytic proteins to establish its infection in plants. *The Plant Journal*, 101, 384–400.

Wu, G., Jia, Z., Ding, K., Zheng, H., Lu, Y., Lin, L. et al. (2022) Turnip mosaic virus co-opts the vacuolar sorting receptor VSR4 to promote viral genome replication in plants by targeting viral replication vesicles to the endosome. *PLoS Pathogens*, 18, e1010257.

Wylie, S.J., Adams, M., Chalam, C., Kreuze, J., López-Moya, J.J., Ohshima, K. et al. (2017) ICTV virus taxonomy profile: *Potyviridae*. *Journal of General Virology*, 98, 352–354.

Xiang, Y., Lyu, R. & Hu, J. (2023) Oligomeric scaffolding for curvature generation by ER tubule-forming proteins. *Nature Communications*, 14, 2617.

Xue, M., Arvy, N. & German-Retana, S. (2023) The mystery remains: how do potyviruses move within and between cells? *Molecular Plant Pathology*, 24, 1560–1574.

Zeng, H., Wang, S., Zhou, T., Zhao, F., Li, X., Wu, Q. et al. (2018) ComplexContact: a web server for inter-protein contact prediction using deep learning. *Nucleic Acids Research*, 46, W432–W437.

Zhang, H., Yuan, Y., Xing, H., Xin, M., Saeed, M., Wu, Q. et al. (2023) Genome-wide identification and expression analysis of the *HVA22* gene family in cotton and functional analysis of GhHVA22E1D in drought and salt tolerance. *Frontiers in Plant Science*, 14, 1139526.

Zhang, Q., Wen, Z., Zhang, X., She, J., Wang, X., Gao, Z. et al. (2023) RETICULON-LIKE PROTEIN B2 is a proviral factor co-opted for the biogenesis of viral replication organelles in plants. *The Plant Cell*, 35, 3127–3151.

SUPPORTING INFORMATION

Additional supporting information can be found online in the Supporting Information section at the end of this article.